

Copyright©

by

Alberto Orlando

2013





UNIVERSITÀ  
DEGLI STUDI  
DI PADOVA

UNIVERSITA' DEGLI STUDI DI PADOVA  
**Dipartimento di Ingegneria Industriale DII**  
Corso di Laurea Magistrale in Ingegneria Meccanica

**CHARACTERIZATION OF THE IMPACT OF RELEVANT  
PROCESS PARAMETERS ON THE HEAT TRANSFER  
AND THE RESULTING MECHANICAL PROPERTIES  
USING MULTI-PHASE STEEL GRADES**

Influenza dei parametri di processo sullo scambio termico e sulle  
proprietà meccaniche risultanti nello stampaggio a caldo di acciai  
multifase

*Relatore: Prof.ssa Stefania Bruschi*

*Laureando: ALBERTO ORLANDO*  
*Matricola: 1013823*

Anno Accademico 2012 – 2013



*To my parents...*



## **Acknowledgements**

I would like to heartily thank Prof. Marion Merklein who gave me the opportunity to perform my Master Thesis at the Lehrstuhl für Fertigungstechnologie, in Erlangen and my tutor, Mr. Thomas Svec, for his help, advices and teachings.





# **Characterization of the Impact Process Parameters on the Heat Transfer and the Resulting Mechanical Properties using Multiphase Steel Grades**

Alberto Orlando

Master Degree in Mechanical Engineering

Università degli Studi di Padova, March 2013

Supervisor: Stefania Bruschi

## **Abstract**

Currently, since automotive industries are obliged to follow severe crash regulations and even increasingly severe antipollution laws, huge efforts are undertaken in order to improve, on one hand, crashworthiness and, on the other hand, fuel consumption, strictly related to carbon dioxide production.

To meet this target, it is necessary to produce, while struggling against two conflicting requirements, lighter designs and, at the same time, more resistant vehicles. That is why new materials need to be investigated in order to meet as best as possible these targets.

Surprising results have been obtained using the widely-used boron-manganese quenchable steel, 22MnB5. Results have shown that if it is cooled down quickly enough, a very strong and hard martensitic structure can be developed, with an ultimate tensile strength up to 1500 MPa. This steel grade is very suitable for passenger compartment to resist deformation and prevent intrusion. By contrast, though, the elongation capability is very poor. Therefore, this kind of steel, after quenching treatment, is not suitable for energy management zone, like the trunk and engine compartment, which must meet the requirement of absorbing crash energy by deformation. At the same time, several part of the car body do not need an extreme strength, so different materials might be used.

Here comes the need for new technologies and materials with different properties compared to the ones of the much-explored quenchable steel grade 22MnB5. That is why the investigation into tailored tempering applied to advanced high strength steels such as Dual Phase and Complex Phase has become even more interesting. Since these

new steel grades may show better elongation and better response to tailored properties, it would be possible to satisfy the crucial requirements of crashworthiness mentioned above.

In the field of hot forming processes and, more precisely, tailored hot stamping, the characterization of Dual Phase and Complex Phase steels has been carried out, both varying quenching temperature on one part of the tool and contact pressure, in order to achieve locally adjusted properties. This work is aimed at calculating experimentally the heat transfer coefficient between the dies and the blank during quenching. Additionally, the features developed in the transition zone, where the steel changes its properties because of the different applied boundary conditions, namely water cooled high conductivity and heatable low conductivity die steel.

The steel grades analyzed in this work are the cold rolled DP-K 45/78 hot dip galvanized zinc coated and the hot rolled CP-W 800 electrolytically galvanized zinc coated, both marketed by ThyssenKrupp Steel Europe.

## **Table of Contents**

Acknowledgements.....	vii
Abstract.....	ix
Table of Contents.....	xi
List of Tables.....	xiii
List of Figures.....	xv
<b>CHAPTER 1</b>	<b>17</b>
1.1 Motivation.....	17
1.2 Aim of the work.....	19
<b>CHAPTER 2</b>	<b>21</b>
2.1 Classification of automotive steels.....	21
2.2 Advanced High Strength Steels (AHSS).....	23
2.3 Influence of alloying elements.....	27
2.4 Hot Forming.....	32
2.5 Tailored Hot Forming for tailored mechanical properties.....	36
2.6 Heat Transfer.....	39
2.7 Heat Transfer during Press Hardening Processes.....	43
2.8 Effect of Plastic Deformation on Material Properties at High Temperature.....	47
<b>CHAPTER 3</b>	<b>49</b>
3.1 Steel Grades Investigated.....	49
3.2 Description of the Procedure carried out during the Work.....	51
3.2 Press Hardening Experiments and HTC Evaluation.....	53
3.3 Micro-Hardness Tests.....	58

3.4	Metallographic Analysis .....	60
3.4	Tensile Tests .....	61
<b>CHAPTER 4</b>		<b>65</b>
4.1	Influence of Process Parameters on Heat Transfer .....	65
4.2	Characterization of the Developed Microstructure .....	71
4.3	Metallographic Analyses .....	76
4.4	Evaluation of Mechanical Properties .....	79
<b>CHAPTER 5</b>		<b>85</b>
5.1	Outlook .....	85
References .....		87

## List of Tables

<b>Table 1.</b> Chemical composition of the steel grades analyzed in this work, ThyssenKrupp Steel Europe (Downloaded: December 2012a,b).....	50
<b>Table 2.</b> Mechanical properties of the steel grades analyzed in this work, ThyssenKrupp Steel Europe (Downloaded: December 2012a,b).....	50
<b>Table 3.</b> Tool and parameter settings for determination of the effect of the process parameters on the resulting material properties.....	55
<b>Table 4.</b> Ranges of temperature actually chosen in dependency of the tool temperature.	56
<b>Table 5.</b> Flow curve's legend of Figure 28.....	84



## List of Figures

<b>Figure 1.</b> Relationship between tensile strength and total elongation for various steel grades at room temperature. (Source: www.autospeed.com) .....	22
<b>Figure 2.</b> The body-in-white of the new Volkswagen Golf model year 2012 is more than 23 kg lighter than its predecessor, due in part to the intensive use of high- and ultra-high-strength steels; moreover it awarded 5-Star Euro-NCAP. (source: www.volkswagen.de) .....	23
<b>Figure 3.</b> Phase formation in dependency of the followed cooling route. ....	24
<b>Figure 4.</b> Influence of the major alloying elements on the TTT diagram. ....	30
<b>Figure 5.</b> Hot stamping processes, (a) depicts the direct hot stamping process, and (b) the indirect hot stamping process, Karbasian & Tekkaya (2010). ....	33
<b>Figure 6.</b> Typical mechanical properties and microstructure of 22MnB5 steel grade, in as-delivered and hot stamped conditions, Karbasian & Tekkaya (2010). ....	34
<b>Figure 7.</b> B-pillars with tailored properties. On the left side, tailored tempering technology was used; on the right tailored welded blank was realized, Karbasian & Tekkaya (2010). ....	37
<b>Figure 8.</b> Real surface of contact between blank and die. ....	45
<b>Figure 9.</b> Experimental route carried out during the present work. ....	52
<b>Figure 10.</b> Principles of the lower part of the quenching tool used during the press-hardening experiments. ....	53
<b>Figure 11.</b> Specimen ready for being inserted into the furnace. ....	54
<b>Figure 12.</b> Facilities used during the press-hardening tests. Close-up, the Lasco <sup>®</sup> press is visible; the furnace is on the right side of the picture. ....	57
<b>Figure 13.</b> Parts being cut from the processed specimen in order to perform hardness measurement HV0.1. ....	58
<b>Figure 14.</b> Fischerscope <sup>®</sup> HM200 used to perform hardness measurements. ....	59
<b>Figure 15.</b> Embedments ready for metallographic analyses. The small ones are for heated and cooled side, the big ones are for the transition zone. ....	60
<b>Figure 16.</b> Dimension of the specimen used for tensile tests. ....	61
<b>Figure 17.</b> Tensile test machine Zwick/Roell <sup>®</sup> ZMART.PRO and CCD camera. ....	62
<b>Figure 18.</b> a) stochastic pattern of a specimen during a tensile test; b) major strain calculated by means of the ARAMIS <sup>®</sup> system .....	63
<b>Figure 19.</b> Heat transfer coefficient calculated experimentally. a) Dual phase steel; b) complex phase steel. ....	67
<b>Figure 20.</b> Heat transfer coefficient between the dual phase specimen and tool as a function of the temperature of the blank in dependency of the tool temperature and contact pressure. From the top to the bottom, tests with heated tool at room temperature, 400 °C and 500 °C are depicted. ....	69
<b>Figure 21.</b> Heat transfer coefficient between the complex phase specimen and tool as a function of the temperature of the blank in dependency of the tool temperature and contact pressure. From the top to the bottom, tests with heated tool at room temperature, 400 °C and 500 °C are depicted. ....	70

<b>Figure 22.</b> Results of hardness tests HV0.1.(a) dual phase results; (b) dual phase results. .....	73
<b>Figure 23.</b> Characterization of the transition zone between heated and cooled part by hardness measurements on the specimen. (a) dual phase steel; (b) complex phase steel.	75
<b>Figure 24.</b> Metallographic analyzes of the developed microstructure in the cooled and heated zone as well as in the transition zone of the dual phase steel, in dependency of tool temperature shown exemplarly for $p_c = 20$ MPa. Magnification 2000x. LOM images. ..	77
<b>Figure 25.</b> . Metallographic analyzes of the developed microstructure in the cooled and heated zone as well as in the transition zone of the complex phase steel, in dependency of tool temperature shown exemplarly for $p_c = 20$ MPa. Magnification 2000x. LOM images. .....	78
<b>Figure 26.</b> Mechanical properties of the dual phase steel grade investigated in the present study. ....	81
<b>Figure 27.</b> Mechanical properties of the complex phase steel grade investigated in the present study. ....	82
<b>Figure 28.</b> Exemplary flow curves at 20 MPa showing the behavior of the dual phase and complex phase steel under different temperature conditions. ....	84



# Introduction

## 1.1 Motivation

The average weight of vehicles is constantly increasing due to the introduction of safety and comfort devices, like Anti-Block Systems, air bags, navigation systems, air conditioning and entertainment systems. That is why car constructors must deal with the issue of limiting the weight of vehicles in order to offer appealing and better performing products to the final consumer and, at the same time, observe severe anti polluting regulations while maintaining reasonable production costs.

Neglecting driving-style, less fuel consumption can be achieved by operating on different main aspects, such as:

- improvements on engine, powertrain and tire efficiency;
- improvements on vehicle aerodynamic;
- vehicle weight reduction.

Manufacturing engineering is focusing even more on optimized body-in-white (BiW), aiming at reducing a car's weight. It is important to note that 100 Kg of weight reduction would decrease fuel consumption by 0.35 liters for 100 Km, Helms & Lambrecht (2006),

or, as mentioned by Galán *et al.* (2012), 10% of weight reduction will improve the fuel consumption of 5.5 %. That is the reason why lightweight design has gained importance in automotive industry. At the same time, crash performance should not be negatively affected, in order to meet safety test defined by the Euro-NCAP and USA-NCAP.

Vehicle weight reduction can basically be obtained by different approaches: one possibility is using low density materials such as aluminum, magnesium, titanium, plastics and composite materials combined to steel; another is using Ultra High Strength Steels (UHSS), characterized by high strength-to-specific gravity ratio, Mori *et al.* (2005), which can lead to an appreciable material saving and, consequently, to a substantial weight decrease.

Both of these ways could lead to appreciable mass saving, but it is necessary to bear in mind that the best optimization is achieved by redesigning the chassis from scratch and not simply replacing the old material with a new one. On one hand, aluminum, magnesium and titanium alloys are affected by a low formability at room temperature because of the hexagonal lattice crystal structure; the use of elevated temperatures can induce a noticeable formability increase but the price of titanium is still too high, which militates against its wide diffusion, Neugebauer *et al.* (2006). Plastics have very low strength, compared to steel, and could be used just on limited zones of the car body but regarding the interesting word of the composite materials, many technical issues have yet to be solved before these materials can be widely used in automotive industry, Mangino *et al.* (2007). On the other hand, the use of Ultra High Strength Steel can lead to remarkable results. Despite how it is affected, using cold forming processes, by a low formability, it dramatically improves at high temperature, especially above re-crystallization temperature.

If non-ferrous alloys are going to be used, the combined use with steel is mandatory; at the same time, connection/joining issues between steel and other alloys, lead to more complex assembly processes compared to “pure” steel manufacturing. In addition, taking into account not only the material’s cost but also the assembly difficulties, the solution involving just steel in the BiW still remains the cheapest and the more feasible option

Field *et al.* (2007). Furthermore, results of the consortium ULSAB (Ultra-Light Steel Auto Body), as a matter of fact, demonstrate UHSS suitability for meeting the strict requirements in future automotive industries, such as reducing the mass, easy forming and fulfilling the energy absorption requirements. As a result of these studies, a remarkable car body structure which weights 36 % less than benchmarked vehicles, has been designed and, surprisingly, successfully fulfilled all crash requirements, American Iron and Steel Institute (downloaded: December 2012).

## **1.2 Aim of the work**

So far, the most examined and used material in automotive industry Ultra High Strength Steel has been the 22MnB5 steel grade, which has led to impressive results thanks to its impressive temperability. Continuous investigation in achieving better formability without losing high strength, leads to the study of different materials and different heat treatments. For this reason, the aim of this work is to characterize, by means of hardness measurements, metallography analyses and tensile tests, of less-investigated multi-phase steel grades. In varying the quenching pressure and punch-die temperature only in a delimited area of the tool, manufacturing components with locally adjusted mechanical properties is practicable. Moreover, since different tool steel grades, which exhibit different thermal conductivity, are employed, it is possible to characterize their influence on the resulting properties after quenching. Additionally, no deformation of the blank is assumed to take place during the press hardening experiments.

The steel grades analyzed in the present study are the cold rolled DP-K 45/78 hot dip galvanized zinc coated and the hot rolled CP-W 800 electrolytically galvanized zinc coated, both marketed by ThyssenKrupp Steel Europe.



# Literature Review

## 2.1 Classification of automotive steels

In order to classify the automotive steel sheets, several ways might be pursued. The list below summarizes a common classification, according to WorldAutoSteel (downloaded: December 2012).

Classification by metallurgical designation:

- Low-strength steels: interstitial-free (IF) and mild steels
- Conventional high-strength steels: carbon-manganese (CMn), bake hardenable (BH), interstitial free high strength (IF-HS) and high strength low-alloy steels (HSLA)
- Advanced-high-strength steels (AHSS): dual phase (DP), transformation induced plasticity (TRIP), complex phase (CP) and martensitic steels

Classification by mechanical properties, namely ultimate tensile strength (UTS):

- Low-strength steels (LSS): UTS < 270 MPa
- High-strength steels (HSS): UTS 270 - 700 MPa
- Ultra-high-strength steels (UHSS): UTS > 700 MPa

Figure 1 highlights the mechanical properties of currently used steels. Total elongation and ultimate tensile strength are rival features. Looking at the figure it is noticeable that low strength steels can stand broad elongation, namely better formability; on the other hand, ultra-high strength steels are affected by lower formability.

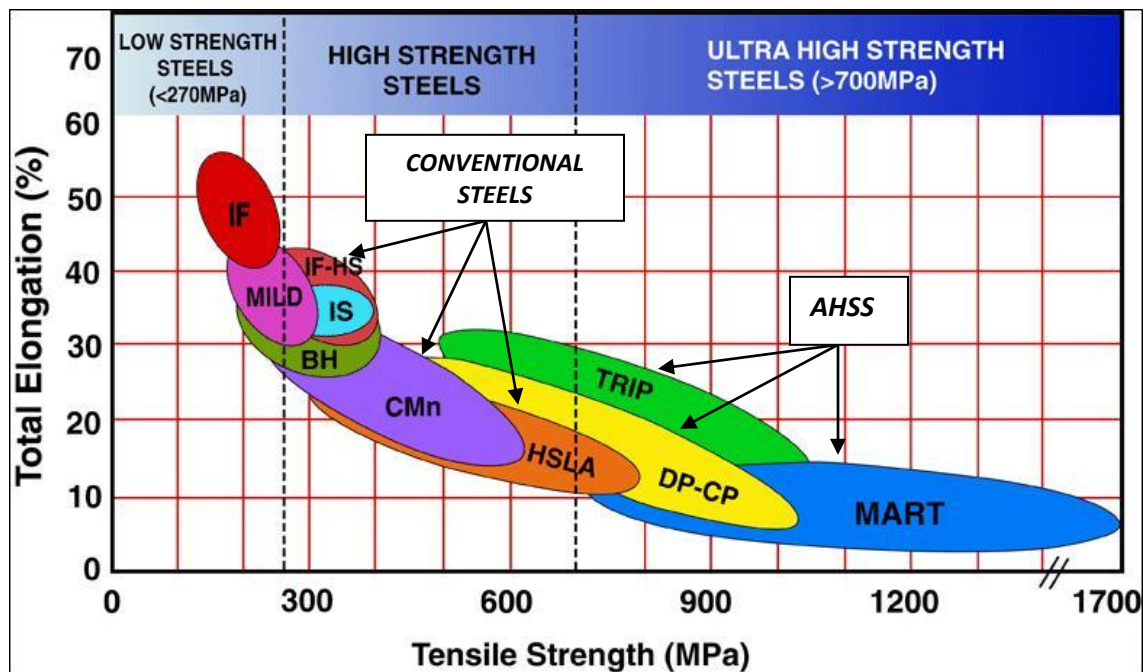


**Figure 1.** Relationship between tensile strength and total elongation for various steel grades at room temperature. (Source: [www.autospeed.com](http://www.autospeed.com))

In addition, it is also important to underline that properties can differ considering hot rolled or cold rolled steel sheets; even coating procedure subject the base metal to different thermal cycles that influence the final properties.

## 2.2 Advanced High Strength Steels (AHSS)

Conventional high strength steels (HSS) are hardened by solid solution, precipitation or grain refinement, while advanced high strength steels are hardened by phase transformation, and their microstructure contains ferrite, martensite, bainite and/or retained austenite. These steels, as depicted in Figure 1, have an impressive strength but a poor elongation (i.e. formability) at room temperature; they are very suitable for crash relevant parts, especially those which are supposed to prevent intrusion into the passenger compartment. Furthermore, AHSS are superior in strength and ductility combination compared to conventional HSS, which means superior crash energy dissipation, improved safety and, at the same time, reducing weight.



**Figure 2.** *The body-in-white of the new Volkswagen Golf model year 2012 is more than 23 kg lighter than its predecessor, due in part to the intensive use of high- and ultra-high-strength steels; moreover it awarded 5-Star Euro-NCAP. (source: [www.volkswagen.de](http://www.volkswagen.de))*

One important aspect to bear in mind is that AHSS are performance based steel grades and they are named and marketed according to metallurgical type and minimum tensile strength: for instance, CP-W 800 means complex phase steel with a minimum ultimate tensile strength of 800 MPa. Last but not least, chemical composition may vary

appreciably from one supplier to another and/or batch to batch. For this reason the tensile properties may match but other parameters such as weldability and elongation might not be the expected ones. Furthermore, it may happen that mills deliver steels that exceed the requirement so the formability and the tool wear during forming will not be accurately predictable, Xiaodong *et al.* (January 2013), Shaw & Zuidema (2001).

Generally, in order to produce steel grades with different peculiarities, it is possible to start the process from a temperature above austenite transformation, and following different cooling patterns, different phases in the same material are feasible. Thus, a fast cooling down may lead to a complete martensitic structure, on the other hand, slower and more complex cooling rate may lead to a mix of ferrite, bainite and martensite; retained austenite is formed when martensite start temperature is below room temperature. By means of this process, it is possible to obtain double phase, transformation induced plasticity, complex phase and martensitic steels. Figure 3 depicts the process mentioned above.

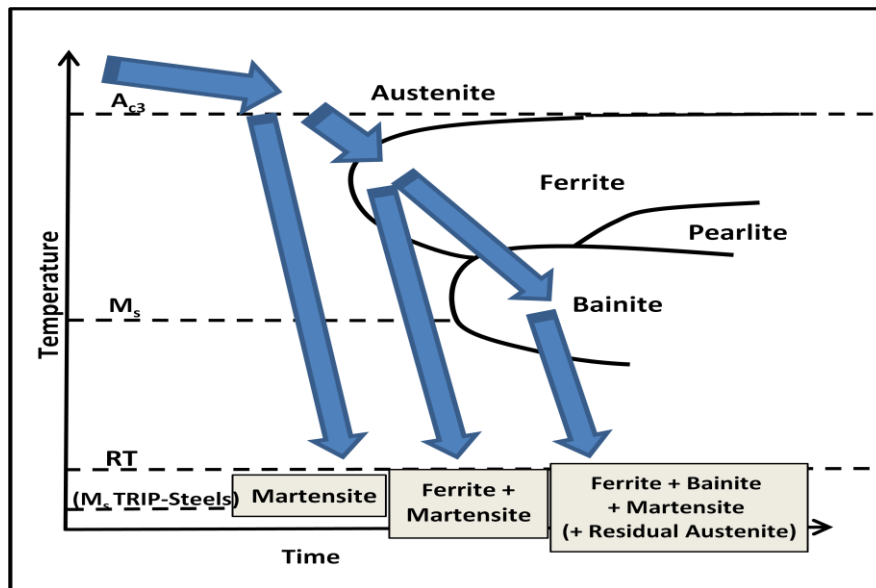


Figure 3. Phase formation in dependency of the followed cooling route.



In the following part, a short summary about these steels is given.

### Dual Phase steels (DP)

The term Dual Phase comes from the light optical microscopy (LOM) description. In such a way, it is possible to appreciate an high formable ferritic matrix, which allows wide strains during tensile tests, Rudiono & Tomota (1997), with a martensitic second phase, present in form of islands at the grain boundaries, providing a better strength to the base ferrite, Bleck *et al.* (2004). Normally the content of martensite varies between 5 % and 20 %, and the tensile strength ranges from 500 to 1100 MPa, ThyssenKrupp Steel Europe (downloaded: December 2012). DP steels are characterized by low yield strength, a high work-hardening ratio, a high bake hardening value, no yielding and no room temperature aging and are widely used in car components that require high strength, good crashworthiness and high formability, Galán *et al.* (2012), such as wheels, bumpers and other reinforcements. The basic composition of DP steel is C and Mn; sometimes some Cr and Mo are added to enhance hardenability. DP steel is also called “partially martensitic steel” when the martensite volume fraction exceeds 20 %.

### TRIP steels

TRIP steels are composed mainly by a ferritic-bainitic matrix which contains martensite and, from 5 % to 15 % of retained austenite due to the martensite start temperature ( $M_s$ ) being lower than room temperature. Retained austenite provides high strain-hardening: the strength of these steels ranges from 600 to 800 MPa. Moreover they exhibit an excellent uniform elongation, ThyssenKrupp Steel Europe (downloaded: Januar 2013), Galán *et al.* (2012). During the forming process, retained austenite can transform into martensite (TRIP-effect), Bleck *et al.* (2004). Silicon is the key element for the formation of retained austenite, but it is undesirable when making steel sheets with high surface quality.

### Complex Phase steels (CP)

CP steels have a chemical composition made by a balance of ferrite, bainite, martensite and precipitation hardening phases in the microstructure, ThyssenKrupp Steel Europe (downloaded: December 2012). It might be observed that the phase composition is similar to the TRIP steels, except that CP steels have no retained austenite. With hard phases like martensite and bainite and some help from precipitation hardening, the ultimate tensile strength of CP steel ranges from 800 to 1000 MPa, which makes the steel excellent for making anti-crash rods, bumper and B pillar. Compared to DP steels, CP steels have significantly higher yield strength values at equal ultimate tensile strength levels. After hot forming, it is possible to achieve strengths of up to  $1200 \text{ N}\cdot\text{mm}^{-2}$  Neugebauer *et al.* (2006).

### Martensite steels (M)

Excellent hardenability can be obtained in steels when enhancing the contain of carbon, manganese and boron. These kinds of steels have been widely used for non-isothermal hot forming and, if the cooling rate is sufficiently fast, they may achieve tensile strength up to 1500 MPa and uniform elongation of 5-6 %, thanks to a stiff martensitic structure leading to the so called martensitic steels, Merklein & Svec (2012). After heating in the furnace, the hot forming process takes about 15 to 25 seconds, Xiaodong *et al.* (Downloaded: January 2013), Merklein & Lechler (2008).

The most common quenchenable steels are the USIBOR 22MnB5, marketed by AcelorMittal and the MBW series, marketed by ThyssenKrupp. Martensite steel is the highest in strength for auto-making and suits the needs of crash deformation resistance components such as a car's passenger compartment.

### 2.3 Influence of alloying elements

Each alloying element in steel has a substantial effect. For this reason, it is of paramount importance to understand their actions and interaction. Alloying elements and cooling rates are crucial when aiming to control accurately the phase transformations in order to reach adequate mechanical properties. The most important elements influencing hardenability, ductility and phase transformation are described in the following part, Ph.D. Dissertation, Hot Stamping of High Strength Steels, Naderi (2007); Hofmann *et al.* (2009).

#### Carbon

Carbon is the most influential element in steel. Its percentage can vary up to 2.06 %; beyond this percentage, the alloy changes properties and is called cast iron. Steel hardness and strength increase as long as the carbon content increases up to about 0.85 %; on the other hand, weldability and ductility decrease while increasing carbon content. Furthermore, carbon content enhances temperability, namely the TTT diagram shifts to the right, delaying the decomposition into ferrite, bainite and pearlite. Consequently, the critical cooling rate is decreased as well as  $M_s$  temperature.

#### Boron

Adding small percentages of boron, e.g. from 10 to 30 ppm, it is possible to enhance hardenability because of the boron's ability to inhibit the nucleation of ferrite. Similar to the carbon effect, the TTT diagram shifts to the right.

### Sulfur

This element decreases ductility and resilience especially at high temperatures because of the formation of ferrous sulfur, responsible for the hot shortness. This phenomenon is more critical in the transverse rolling direction.

### Phosphorus

Phosphorus increases strength, hardness and corrosion resistance; on the other hand it decreases ductility and resilience, especially in quenched and tempered high carbon steels. Furthermore, it increases the austenitization temperature and, similar to sulfur, it could be responsible for hot shortness. For this reason, it is necessary to restrict the phosphorus content to less than 0.05 %.

### Manganese

Manganese is always present in steel (about 0.3 %) because it provides a de-oxidizing action. Furthermore it enhances formability since it avoids the formation of ferrous sulfur, responsible for the hot shortness. Higher percentages (beyond 2 %) are present in modern AHSS, in order to provide better hardenability; and at the same time, the weldability and ductility decrease; this effect, though, is less appreciable than increasing carbon content. Moreover, increasing manganese content provokes the  $M_s$  temperature to decrease.

### Titanium

Titanium is both used for retarding grain growth and minimizing inter-granular corrosion. Furthermore, it induces the sulfides to be globular instead of acicular, providing enhanced ductility and toughness in the transverse direction.

## Chromium

Chromium is a quite a cheap element and is added in order to provide better oxidation resistance. Contents of 11 % are typical of stainless steel, which has a very marked resistance to corrosion in comparison to other steels. When added to low alloy steels, it can increase the heat treatment response, thus improving hardenability and strength. In addition, chromium enhances temperability and decreases the  $M_s$  temperature.

## Molybdenum

Molybdenum is an expensive element. It forms stable carbides. When added to low alloy steels, molybdenum improves the high temperature strength and hardness. At the same time, it enhances the temperability.

## Vanadium

Vanadium strongly stabilizes carbides. It increases the yield strength and the ultimate tensile strength of carbon steels by precipitation strengthening and grain refinement.

## Silicon

Silicon acts as a deoxidizing agent in the melting of steel and also contributes to hardening the ferritic phase in steel. For this reason, silicon killed steels are somewhat harder and stiffer than aluminum killed steels. Temperability is negatively affected when adding silicon.

## Aluminum

As well as silicon, aluminum is used as a de-oxidative agent. It is also used in nitrided steels because of its tendency to form very hard nitrides. Moreover, aluminum negatively affects temperability.

Figure 4 helps to figure out the effect on the TTT diagram of the most important alloying elements in steel.

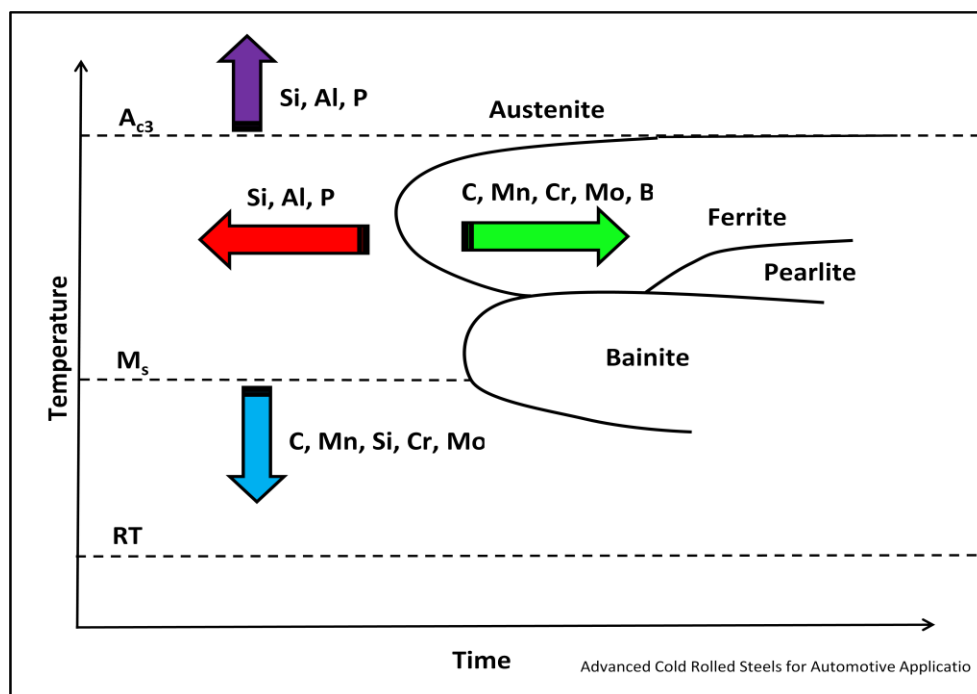


**Figure 4.** Influence of the major alloying elements on the TTT diagram.

It is possible, though, to mix the above mentioned elements in order to obtain the optimum condition between strength and ductility. For instance, the Authors Vandeputte *et al.* (2001) proposed to decrease the carbon content to between 0.05 % and 0.1 %, and, in doing so, losing strength but gaining in ductility, adding chromium and boron as

hardenability enhancers. The cold formability of such steel is good and, after hardening, it has high mechanical properties.

Advanced high strength steels, due to their high strength, suffer from poor formability in the delivered state. Thus, it is necessary to use properly tuned forming processes at high temperature.

The Authors Neugebauer *et al.* (2011) pointed out the crucial influence of alloying elements such as C, Si, Mn, Cr, Mo, B and Ti in several advanced high strength steels CCT diagrams (Si is especially supposed to enhance the ferrite transformation) and discussed the resulting mechanical properties. It is interesting to notice that, considering a quenching cooling rate at  $20 \text{ K}\cdot\text{s}^{-1}$ , DP 1000 and CP-W 800 turned out not to be suitable sheet alloys to be used in hot forming because of their poor hardenability. By contrast, the manganese-boron 22MnB5 and the air hardenable LH800 steel grades showed a good hardenability in the same conditions investigated.

## 2.4 Hot Forming

Nowadays, ultra high strength steels have become very common in the automotive industry, due to their impressive strength, although this feature leads to high forming stresses and important spring-back. Hot forming has become established as one of the most important technologies for body-in-white since it leads to the possibility of forming accurate high strength parts with lower load on tools.

Hot forming is a non-isothermal process in which the blank is simultaneously formed and quenched in one single step. In a typical hot forming route, the as-delivered material is heated up above recrystallization temperature and simultaneously formed and quenched in order to achieve high mechanical properties.

Such a process is present in two main different variants, namely the direct and indirect hot forming method.

In direct hot forming processes, see Figure 5 (a), after blanking, the as-delivered material is heated up in a furnace in order to obtain homogeneous austenitic microstructure; oxide scale formation occurs once the blank is in contact with air. For this reason, hot forming blanks are normally provided with an Al-Si coating that is very stable at high temperature, in order to prevent scale formation, Merklein & Lechler (2008). Once the blank has been dwelled for at least 5 minutes, it must be quickly transferred to the press where it is formed and quenched at the same time between actively water-cooled dies.

On the other hand, the indirect hot forming process, see Figure 5 (b), is characterized by a nearly complete cold pre-forming of the uncoated blank, normally until 90 to 95 % of its final geometry. Subsequently the blank is heated up and transferred to the press for a quenching and calibration operation under inert atmospheric conditions. Afterwards, the surface has to be post-processed by various methods to improve its quality, Merklein & Lechler (2008).



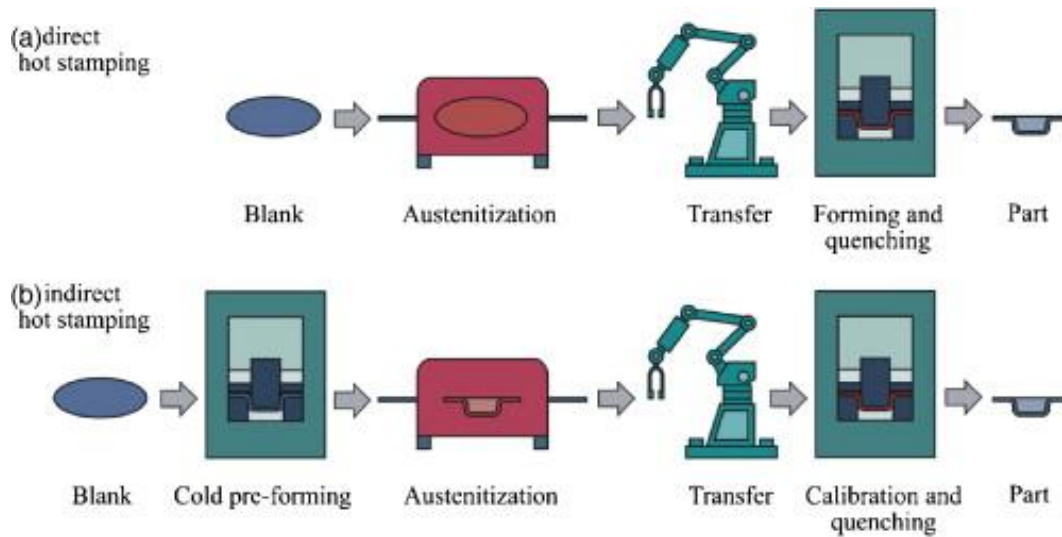


**Figure 5.** Hot stamping processes, (a) depicts the direct hot stamping process, and (b) the indirect hot stamping process, Karbasian & Tekkaya (2010).

Deformation during hot stamping is carried out at high temperature, by means of the activation of additional glide planes in the austenite, which has a face-centered cubic (FCC) crystal lattice structure. Martensite has a body-centered tetragonal (BCT) unit cell, which is a rectangular prism slightly elongated along one of its principal axes. It does not have as many slip plane as does the austenite; moreover, the carbon is allowed to be in interstitial positions. For these reasons, martensite is extremely hard and brittle. Figure 6 shows the typical flow curve and the microstructure changes during the hot stamping process. The ductile material in as-delivered becomes very strong and brittle after the quenching treatment, because of the phase transformation to martensite.

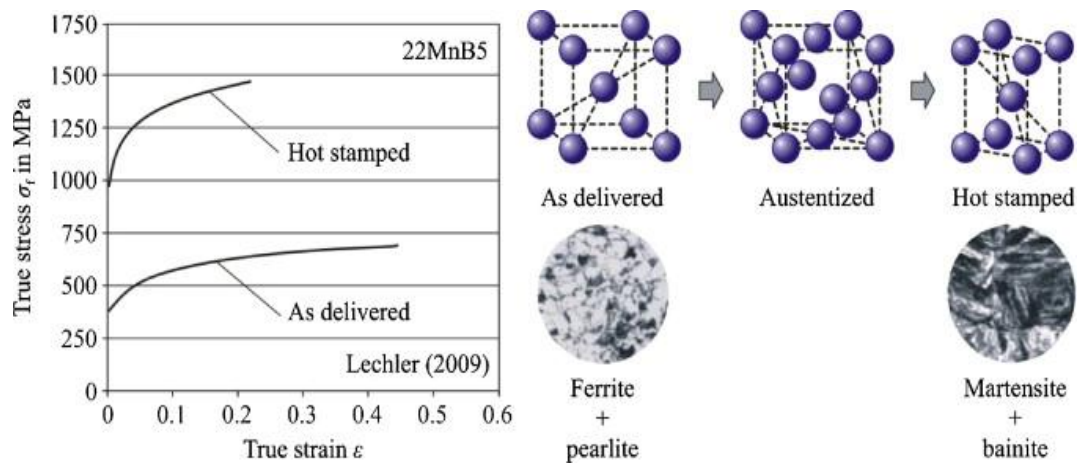


**Figure 6.** Typical mechanical properties and microstructure of 22MnB5 steel grade, in as-delivered and hot stamped conditions, Karbasian & Tekkaya (2010).

Additionally, a phase change from austenite to martensite involves increasing in volume up to 4 %, Kalpakjian & Schmid (2003), Moyer & Ansel (1975), due to the transition from FCC to a BCT lattice structure. Smaller expansions take place also when austenite transforms to pearlite. This issue should be taken into account during forming processes because it, together with the thermal gradients present in a quenched part, it could cause undesirable internal stresses within the body that may cause failures.

The quenchenable steel sheet 22MnB5, with a thickness of 1.75 millimeters, object of recent studies, Karbasian & Tekkaya (2010), shows a ferritic-pearlitic microstructure with low mechanical properties in as-delivered conditions. From the investigation, it turned out that a furnace temperature of 950 °C and a dwell time of 3 minutes was found to be sufficient to gain complete homogeneous austenitic soft structure and, after quenching, to obtain a maximum martensitic content, with a maximum hardness of about 470 HV and no spring-back problems. However, the dwelling time should be matched to the steel grade and the thickness of the blank. The microstructure of a steel alloy can be drastically modified by the use of various heat treatments, i.e. cooling down and/or heating up blanks at different rates in order to achieve desired properties. Thermal treatments induce phase transformations in the steel which deeply influence mechanical

properties such as strength, ductility, hardness and toughness. The effect of the thermal treatment is closely related to the chemical composition, the microstructure and the degree of prior cold work of the steel and, as already mentioned, the cooling and heating rates, moreover, the treatment duration, Kalpakjian & Schmid (2003).

It is crucial to oversee completely the hot forming process in order to guarantee a reliable prediction of the resulting properties, the volume fraction of different phases, the residual stresses and the distortion of the work piece after cooling. FEM analyses are of paramount importance for predicting mechanical properties after the forming process. For this reason, a complex coupled thermo-mechanical model is necessary for consistent results with the real problem, Ghosh & Kikuchi (1988), Neubauer *et al.* (2008), Ph.D. Dissertation, Åkeström (2006), Ph.D. Dissertation, Turetta (2008). Additionally, the imprecise knowledge of the hot stamping process parameters constitutes the major weakness of the process simulation, Neugebauer *et al.* (2006).

The ultra-high strength mechanical properties of hot formed materials have led to their application in chassis components such as A/B-pillar reinforcements, bumpers, door beams, roof rails, and other structural members with high specific strength. Results of ULSAB proved the possibility of achieving remarkable weight reduction when adopting UHSS fulfilling the crashworthiness requirements. In the following part, the main advantages of hot stamping are listed, Neugebauer *et al.* (2006); Ph.D. Dissertation, Naderi (2007):

- excellent shape accuracy of the components, i.e. the possibility of producing ultra-high strength parts without any spring back;
- yield point is reduced up to 60 %, leading to low stress for the forming tools;
- ultimate tensile strength up to 1500 MPa after quenching;
- high elongation at brake during forming process.

These important advantages are of paramount importance in designing cutting-edge parts.

## 2.5 Tailored Hot Forming for tailored mechanical properties

Hot formed components in a fully martensitic state exhibit very high strength but, unfortunately, are affected by a very low level of ductility, which limits their wide use in crashworthiness components. It has been stated that improved crash performances of BiW can be achieved by introducing regions which have good strength and ductility for improved energy absorption, like in engine compartment, trunk and the lower part of the B-pillar. By contrast, parts like the passenger compartment are supposed not to deform considerably and maintain their integrity, to prevent intrusion and, consequently, lethal damages to human beings. Such a technology can be achieved minimizing additional manufacturing steps, Lenze *et al.* (2008), George *et al.* (2012), and, consequently, costs. In order to come up with this issue, different technologies are available such as:

- tailor welded blanks;
- tailored tempering;
- partial austenitization.

In tailored welding, different steels with different features and/or thicknesses can be joined by welding. A challenging alternative seems to be the so-called tailored tempering, during which different features can be achieved by the use of different cooling rates in different areas of the specimen, Karbasian & Tekkaya (2010).

Figure 7 depicts two B-pillars, the left one realized by controlling the cooling rate during quenching, the right one obtained by welding two different steels. It is apparent that the resulting final properties are very similar but the manufacturing process is rather different.

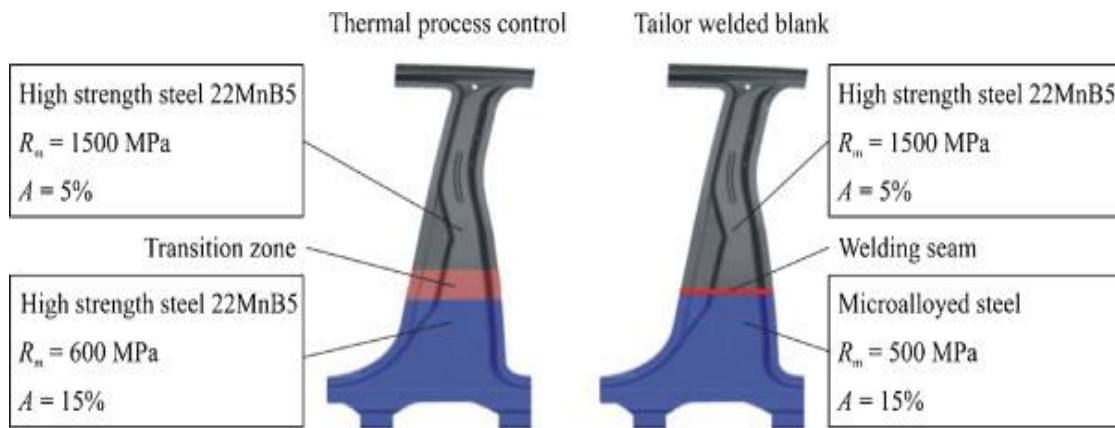


**Figure 7.** B-pillars with tailored properties. On the left side, tailored tempering technology was used; on the right tailored welded blank was realized, Karbasian & Tekkaya (2010).

Partial austenitization consists on heating up only a certain part of the blank below  $A_{c3}$  temperature, causing incomplete austenitization, while the rest of the blank is heated up above  $A_{c3}$ . After quenching, the part will be provided by the ductile zones where the temperature was below austenitization. This process has been studied by the Authors (Stöhr, Lechler, & Merklein, 2009) and turned out to be a practicable way for obtaining tailored properties. Concerning the investigated material boron-manganese 22MnB5 steel, a temperature below  $825 \text{ }^\circ\text{C}$  ensures complete austenitization, as proven by flow behavior and hardness measurements.

Tailored tempering on the 22MnB5 steel has been studied as well George *et al.* (2012), Svec & Merklein (2011), Svec & Merklein (2012), Banik *et al.* (2011), and the use of such a technology has revealed effective in achieving different microstructures, i.e. different material properties on a unique specimen.

Concerning tailored tempering, one effective way to reach tailored properties in a single blank is the differential heating of dies, some zones are kept at low temperature by active water cooling, while other zones are heated from  $300 \text{ }^\circ\text{C}$  up to  $500 \text{ }^\circ\text{C}$ , Svec & Merklein (2011), Svec & Merklein (2012). By increasing the quenching tool temperature in a localized zone, it is possible to reduce the conduction heat transfer between the blank and the die surface, thus decreasing the cooling rate of the blank, while in other zones, the

heat transfer remains at high level, because of the water cooled dies. This will generate localized high strength regions, mainly martensitic, and other region more ductile, composed of daughter phases, e.g. ferrite and pearlite. The selected tool temperature influences the cooling rate and, consequently, the material properties. Particular attention must be paid to the process variables: first and foremost, the cooling rate during quenching which occurs on each zone of the blank, in order to obtain the desired microstructure and thereby the proper strength-ductility match.

Tool thermal conductivity also plays an important role on reaching the desired properties on a hot stamped part, e.g. varying the thermal conductivity of the tool in the range from 7 to 66  $\text{W}\cdot\text{m}^{-1}\cdot\text{K}^{-1}$ , Casas *et al.* (2008), leads to significant changes in the steel features. Further studies revealed that the use of non-ferrous material, such as advanced ceramics, can be used in order to decrease the cooling rate and, consequently, avoid a complete martensitic transformation, Tondini *et al.* (2011).

## 2.6 Heat Transfer

Heat transfer is the physical phenomenon in which heat energy is transferred from a higher temperature body to another one with a lower temperature. This principle is also known as the second law of thermodynamics.

It is well known that heat transfer occurs by three methods:

- convection;
- radiation;
- conduction.

In order to review the difference between these three methods, let us consider the following example. Two bodies are not in contact in a closed, adiabatic room full of air, one at a high temperature, the other one at a lower temperature, both at a higher temperature with respect to the air. At the beginning, if there is any temperature difference between the air and the bodies, convection heat transfer will occur, together with radiation from the bodies to the room. Let us suppose, then, that contact between the two bodies occurs. Consequently the hotter body will lease heat energy to the colder one, with such a process going on until the two bodies and the air reach the equilibrium; namely the two bodies and the air all have the same temperature.

In this simple example, all the heat transfer methods take place. While there is no contact between the bodies, just convection between the air and the bodies, and radiation from the bodies to the room occurs. Afterwards, once the contact between the two bodies is present, conduction is also in effect and, normally, it is the predominant effect.

In the following part, the above mentioned heat exchange methods are presented more in detail.

### Convection

This is the typical heat transfer process in presence of fluids. Gases and liquids have a density-to-temperature dependency, which leads to a more or less orderly fluid flow from high temperature to lower temperature zones. The convection heat transfer process is described by a simple equation:

$$q_{conv} = K_{conv}AdT \quad (1)$$

Where  $q_{conv}$  is the heat transferred by convection per unit of time [W];  $K_{conv}$  is the convection heat transfer coefficient [ $W \cdot m^{-2} \cdot K^{-1}$ ];  $A$  is the heat transfer area [ $m^2$ ];  $dT$  is the effective temperature difference between the surface and the bulk fluid [K].

### Radiation

Radiation is the process by which a body exchanges thermal energy with the surrounding area by electromagnetic waves; no medium and no contact are required. All matter with a temperature higher than absolute zero releases thermal radiation. The so-called Stefan-Boltzmann law describes the phenomenon:

$$q_{rad} = \delta_s F_{12} A (T_1^4 - T_2^4) \quad (2)$$

Where  $q_r$  is the heat transferred by radiation per unit of time [W];  $F_{12}$  is the radiation shape factor from surface 1 to surface 2, no measurement unit;  $\delta_s$  is the Stefan-Boltzmann constant, its value is  $\delta_s = 5.67 * 10^{-8} W \cdot m^{-2} \cdot K^{-4}$ ;  $A$  the radiating area [ $m^2$ ];  $T_1$  is the radiating body temperature [K];  $T_2$  is the surrounding temperature [K].



## Conduction

Conduction is the typical heat transfer process in presence of solids. Transfer of thermal heat is caused by diffusion and collision of particles within the material due to temperature gradient. The conduction heat flux can be definite as follows:

$$q_{cond} = K_{cond}AdT \quad (3)$$

Where  $q_{cond}$  is heat transferred by conduction per unit of time [W];  $K_{cond}$  is the conduction heat transfer coefficient [ $\text{W}\cdot\text{m}^{-2}\cdot\text{K}^{-1}$ ];  $A$  is the heat transfer area [ $\text{m}^2$ ];  $dT$  is the effective temperature difference between two considered points [K].

When the internal conduction resistance is negligible compared to the surface thermal resistance, namely a small Biot number, (for instance a metal sheet due to the very small thickness compared to the other dimensions), the instantaneous thermal flux can be described as follows, Bonacina *et al.* (1989):

$$\alpha A(T_f - T)dt = c\rho VdT \quad (4)$$

Where  $\alpha$  is the interfacial heat transfer coefficient [ $\text{W}\cdot\text{m}^{-2}\cdot\text{K}^{-1}$ ];  $A$  is the actual area where the thermal flux takes place [ $\text{m}^2$ ];  $T_f$  is the temperature of the material in contact with the body [K];  $T$  is the actual temperature of the body [K];  $dt$  is an infinitesimal time step [s];  $c$  is the specific heat of the body [ $\text{J}\cdot\text{kg}^{-1}\cdot\text{K}^{-1}$ ];  $\rho$  is the density of the body [ $\text{kg}\cdot\text{m}^{-3}$ ];  $V$  is the volume of the body [ $\text{m}^3$ ] and  $dT$  an infinitesimal temperature step [T].

The product can also be written as:

$$\dot{q} = \alpha A(T_f - T) \quad (5)$$

This formula is known as Newton's cooling law. The parameter  $\dot{q}$  represents the amount of transferred heat between the two contact surfaces per time unit and  $T$  the actual temperature of the body. As can be noted, the amount of heat transferred is proportional to the difference of temperature between the two body in contact.

Supposing  $\alpha$ ,  $c$  and  $\rho$  to be constant, it is possible to integrate the previous equation and write:

$$T(t) = (T_i - T_f)e^{-\frac{\alpha A}{c\rho V}t} + T_f \quad (6)$$

Where the symbols maintain the same meaning as before and  $T_i$  and  $T(t)$  are the initial and actual temperature of the body [K]. This formula has been widely and successfully used for the heat transfer coefficient experimental evaluation in several works concerning hot stamping processes, some examples being, Bosetti *et al.* (2010), Svec & Merklein (2011), Merklein *et al.* (2008), Merklein & Svec (2012), Karbasian & Tekkaya (2010), Merklein & Lechler (2008).

## 2.7 Heat Transfer during Press Hardening Processes

There are many variables influencing heat transfer between dies and blanks during the hot forming processes. This makes evaluation and comprehension of this phenomenon by no means trivial. At the same time, the heat transfer during hot forming is crucial in order to produce reliable FEM-based models.

Let us consider the heating up in the furnace, in this case convection and radiation take place, at the same time. Afterwards, the blank has to be transferred to the dies, and during this time, convection and radiation through the surrounding air at room temperature occur. When the blank is placed onto the lower die, if gap holders are used, no contact between dies and blank occurs until the dies have been closed. On the other hand, convection through the air takes place and radiation to the air and to the very close lower dies occurs. While the upper dies approaches the blank, the radiation effect for the upper side gains more importance. Once the dies are closed and the contact between blank and dies becomes effective, namely during the actual quenching treatment, conduction plays the main role (Shapiro, 2009), (Neugebauer, Göschel, Rautenstrauch, & Meza-García, 2011).

As proposed by the Authors Tondini *et al.* (2009), heat transfer coefficient (HTC) dependency can be divided into two broad categories:

- system inherent properties, e.g. geometry, materials, thermal properties;
- external system conditions, e.g. applied pressure, contact surface conditions, like roughness and cleanness.

Variables influencing the heat transfer coefficient in hot stamping are briefly discussed below.

Within the first category, different blank material and die geometries could lead to different thermal gradients and, consequently, influence the heat transfer coefficient.

Blank and die geometries influence zones, between punch and blank, in which the contact occurs first; moreover, the geometry affects air flow and heat exchange by radiation.

Shape, roughness, temperature and relative position between blank and dies influence radiation thermal exchange. Furthermore, the factor of view increases between work-piece and dies when the latter one comes closer to the blank and when dies surfaces are parallel to the blank ones, Tondini *et al.* (2009). Thermal properties of the die and work-piece like heat capacity and thermal conductivity, also influence the HTC.

During quenching processes, the surface of the blank never makes perfect contact with the die surface, due to blank oxidation, roughness and possible interspaces between blank and dies. For this reason, heat flux occurs just in discrete spots. This means that the area through which the heat flux occurs is not 'simply connected', Dour *et al.* (2006).

Material Young modulus, of both blank and dies, influences the effective contact area since a low modulus could lead to a greater surface asperity deformation and, consequently, increase the effective contact area. Similarly, a greater pressure between the contact surfaces smooths the roughness, allowing a wider contact area. The Author Madhusudana (1996) proposes, both for plastic deformation and elastic deformation of the asperities, proportionality between true area of contact and applied pressure.

Figure 8 shows the true contact area actually responsible of the heat flux of conduction, very different from the apparent contact area, which can be seen to the naked eye. In the gaps between the contact spots, radiation and convection through the air trapped in those volumes take place. Furthermore, it must be noted that the coating of a blank after annealing in a furnace may result in oxidation and scaling. For these reasons, coating conditions may affect the heat transmission from the blank to the dies, Wang *et al.* (2012).

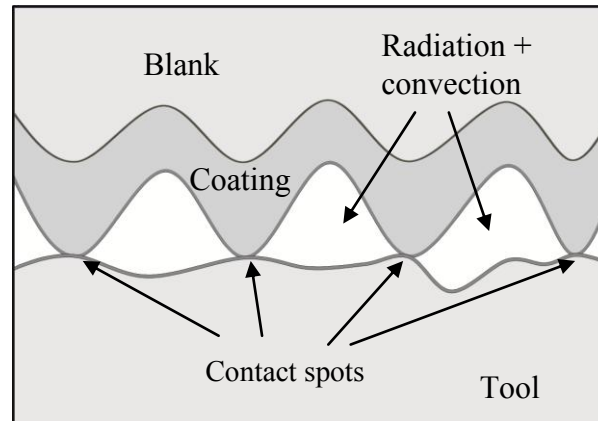


**Figure 8.** Real surface of contact between blank and die.

Experiments carried out in order to identify the heat transfer coefficient at the blank-die interface as function of applied pressure, showed that the heat flux increases with pressure; since the more pressure is applied, the more the peaks are deformed and smoothed, Tondini *et al.* (2009), Bosetti *et al.* (2010), Merklein & Lechler (2008).

Furthermore, if blank zones have a different heat transfer coefficient, gradients of temperature may occur on the blank, leading to internal heat flux, Svec & Merklein (2011). In addition, the amount of heat generation by plastic deformation occurring during forming must be considered to formulate correctly the model of the process, Kang *et al.* (2007).

The thermal conductance can be considered as a comprehensive coefficient, gathering together the conduction, radiation and convection phenomena in a unique thermal conductance coefficient, Svec & Merklein (2011), Wang *et al.* (2012), Bosetti *et al.* (2010).

The heat flux can be described as follows:

$$q_{int} = K_{tot}A(T_B - T_D) \quad (7)$$

Where  $q_{int}$  is the overall heat flux transferred from the blank to the dies per unit of time [W];  $K_{tot}$  is the total heat transfer coefficient, sum of convection, radiation and conduction heat coefficient in parallel [ $W \cdot m^{-2} \cdot K^{-1}$ ];  $A$  is the heat transfer area [ $m^2$ ];  $T_B$  is the actual blank temperature and  $T_D$  is the actual die surface temperature [K]. The formula above mentioned simply collects all the effects of the heat transfer from the blank to the external room and to the dies.

It is worth observing that the heat transfer coefficient during a hot stamping process is not generally constant. It can be assumed constant only in certain ranges of temperature, namely when the heat flux reach a steady state, Svec & Merklein (2011), Wang *et al.* (2012), Merklein & Svec (2012), or between a narrow range of temperatures, Merklein & Lechler (2009).

Since the majority of the steels change their phase during cooling down from high temperature, namely from austenite to martensite or other daughter phases, the variation of enthalpy has to be taken into account when such a phenomenon occurs for a proper description of the problem. The Authors Hasan *et al.* (2011) suggest treating the latent heat like an internal heat source. The latent heat generated from austenite to martensite is  $\Delta H = 6,67 * 10^8 J \cdot m^{-3}$  and the increase of temperature could be calculated in dependency of the amount of austenite transformed into martensite.

Regarding the equation (6), due to the fact that true contact area cannot be determined,  $A$  is assumed to be equal to the apparent area, i.e. equal to the geometrical dimension of the specimens quenched between the contact plates. Moreover, the Authors Merklein & Lechler (2008) and Naderi *et al.* (2008) suggest to use a constant value for the specific heat, equal to  $650 J \cdot kg^{-1} \cdot K^{-1}$ . Since the temperatures are known data coming from the thermocouples, the only unknown parameter is the heat transfer coefficient, which can be calculated thusly:

$$\alpha = -\frac{c_p \cdot \rho \cdot V}{A \cdot t} \ln \left( \frac{T(t) - T_f}{T_i - T_f} \right) \quad (8)$$

Differentiating equation (8) by the time leads to the corresponding cooling rate  $\dot{T}$  of the specimen analyzed:

$$\dot{T} = (T_i - T_f) \left( -\alpha \frac{A}{c_p \cdot \rho \cdot V} \right) e^{-\left( \alpha \frac{A}{c_p \cdot \rho \cdot V} t \right)} \quad (9)$$

The cooling rate so calculated is expressed in  $[\text{K} \cdot \text{s}^{-1}]$ .

## 2.8 Effect of Plastic Deformation on Material Properties at High Temperature

Several studies have been carried out using the 22MnB5 steel grade. The aim was the characterization of the temperature of deformation influence under typical hot stamping conditions. The results showed that the plastic deformation applied at a high temperature increases the internal energy of the material, resulting in a shift towards the right in the TTT diagrams, namely the critical cooling rate required for martensitic transformation for hot stamped parts to  $35 \text{ K} \cdot \text{s}^{-1}$  instead of the  $27 \text{ K} \cdot \text{s}^{-1}$  normally required in absence of deformation, Naderi *et al.* (2008), Ph.D. Dissertation, Naderi (2007), Ph.D Dissertation, Turetta (2008), Merklein & Lechler (2008).





# Procedure

### 3.1 Steel Grades Investigated

This study considers two multi-phase advanced high strength steel grades, supplied by ThyssenKrupp Steel Europe:

- CP-W 800 ZE
- DP-K 45/78 Z

Thickness for both the steel grades is 1.75 mm.

In Table 1 the chemical composition is highlighted for the steel grades being used in this work, ThyssenKrupp Steel Europe (Downloaded: December 2012a,b).

**Table 1.** Chemical composition of the steel grades analyzed in this work, ThyssenKrupp Steel Europe (Downloaded: December 2012a,b).

Steel grade	C max	Mn max	Si max	P max	Cr+Mo max	S max	Nb+Ti max	Al max	V max	B max
DP-K 45/78 ZE	0.18	2.20	0.50	0.04	1.00	0.01	0.15	1.20	-	0.005
CP-W 800 Z	0.12	2.20	0.80	0.04	1.00	0.015	0.15	1.20	0.20	0.005

The dual phase steel is provided with a hot dip galvanized zinc coating, characterized by the typical bright gray color; in contrast, the complex phase steel is provided with an electrolytically galvanized zinc coating, which has a grey color as well, but less bright than the hot dip galvanized one.

In table 3 the mechanical properties for the uncoated steels are shown:

**Table 2.** Mechanical properties of the steel grades analyzed in this work, ThyssenKrupp Steel Europe (Downloaded: December 2012a,b).

Steel grade	Yield strength $R_e$ MPa min.	Yield strength $R_e$ MPa max.	Tensile strength $R_m$ MPa min.	Tensile strength $R_m$ MPa max.	Elongation $A_{80}$ % min.
DP-K 45/78 ZE	450	780	780	900	14
CP-W 800 Z	680	830	800	980	10

At a glance, significant differences can be noted between the two steel grades being studied. The complex phase exhibits higher yield strength and lower elongation compared to the dual phase grade. Moreover, the dual phase has significantly less Si content; this might mean a better temperability. The V present in the complex phase steel increases the strength by precipitation hardening and grain refinement.

As stated by ThyssenKrupp, these steels are developed to meet the automotive industry regulations for weight reduction and safety, thus they are particularly suitable for cold forming operations, although their high strength.

Regarding the quenching response of the steels investigated, some assumptions could be made, if compared to the boron-manganese steel 22MnB5. As reported by the Authors Neugebauer *et al.* (2011), considering a cooling rate of  $20 \text{ K}\cdot\text{s}^{-1}$ , both the complex phase and dual phase steel develop a softer structure compared to the 22MnB5; this mean lower temperability, probably due to the lower carbon content. For this reason, higher cooling rates are mandatory for complex and dual phase steels in order to achieve a martensitic structure after quenching. The lower carbon content probably influences also the maximum UTS achievable after quenching. Therefore, the steel grades investigated in this work will not exhibit as high strength as the 22MnB5.

### **3.2 Description of the Procedure carried out during the Work**

In this chapter the experimental work performed in order to characterize the multiphase steels grades object of the study, is summarized. This will make it easier to understand all the procedure carried out, in order to get an overall picture.

Firstly, the blank was austenitized in the furnace, then manually transferred to the quenching tool and quenched. The temperature profile was recorded from the opening of the furnace to the end of quenching in order to calculate the heat transfer coefficient during quenching, namely when it could be assumed to be almost constant. As already stated, a reliable HTC determination is crucial for the future FE-simulations, Merklein & Lechler (2008). A minimum of three quenching test were performed in order to guarantee repeatability. The same three specimens so processed, were laser cut and analyzed by metallography analysis, hardness measurements and tensile tests. After the experimental work, data analyses were carried out in order to understand the main peculiarities of the steels investigated. Figure 9 helps to understand the overall experimental route.

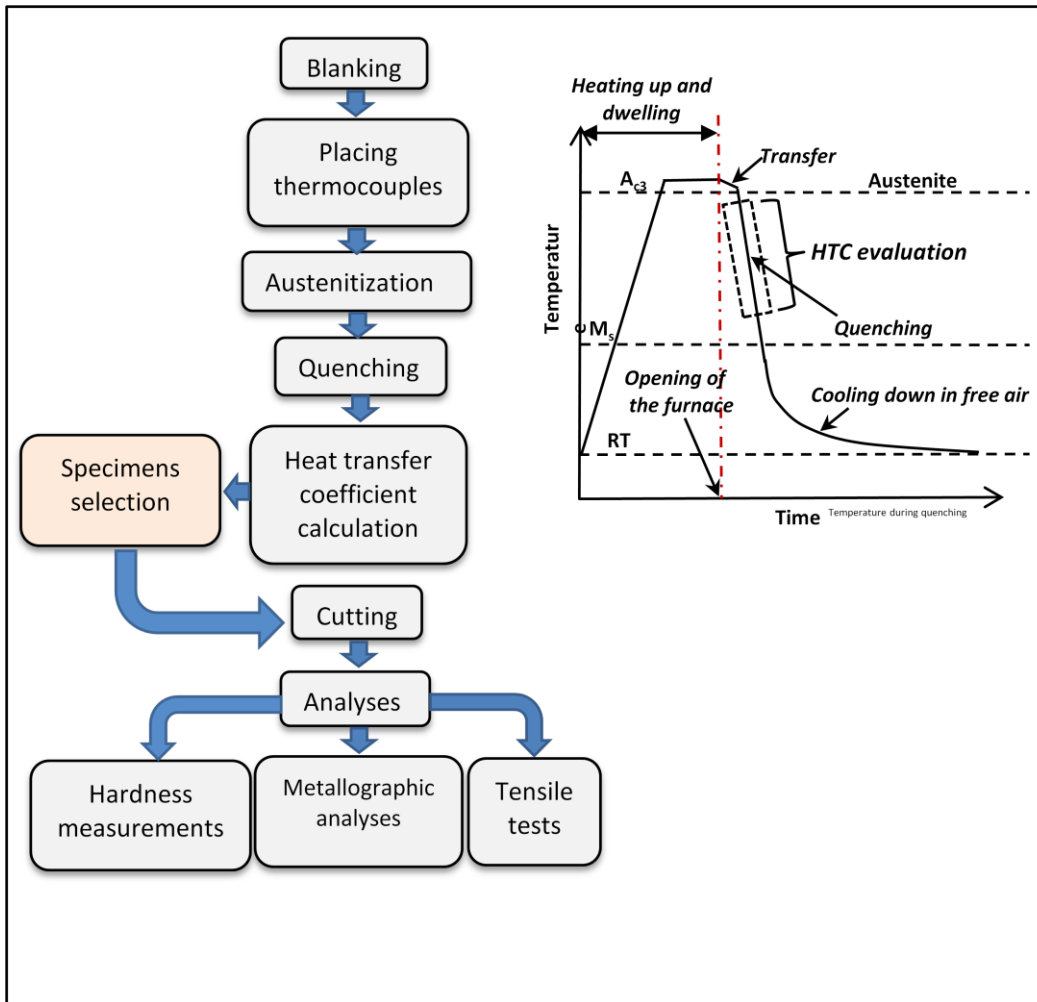
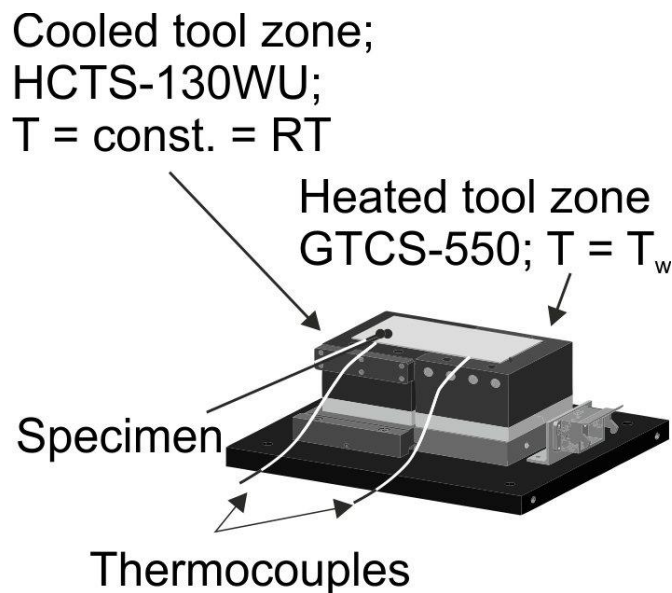


Figure 9. Experimental route carried out during the present work.

### 3.2 Press Hardening Experiments and HTC Evaluation

Quenching operations are dominated by the heat transfer coefficient and influenced by important process parameters. In order to obtain reliable FEM-simulations, it is necessary, first of all, to gain a detailed knowledge of the HTC in dependency of tool temperature and contact pressure.

In order to characterize the heat transfer under process relevant conditions, experiments using a quenching tool in laboratory scale, constructed at the chair of manufacturing technology, University of Erlangen-Nürnberg, were carried out. The quenching tool, as depicted in Figure 10, is separated into active water cooled (HTCS130-WU steel grade) and heated zone (GTCS-550 steel grade), thus allowing the characterization of both pressure and temperature influence and the possible resulting internal heat flux within the blank.



**Figure 10.** Principles of the lower part of the quenching tool used during the press-hardening experiments.

Rectangles sized 100 X 200 mm of both the complex phase and dual phase steel grades were cut by a traditional hydraulic shearing machine. Afterwards, 1.1 mm diameter and about 8 mm deep holes were drilled in all the blanks in the middle of each half of heated and cooled zone, in order to insert Ni/Cr-Ni thermocouples type K (speed of response 0.6 s, correctness  $\pm 1.5$  °C) for instantaneous temperature data acquisition during the press-hardening process as depicted in Figure 11.

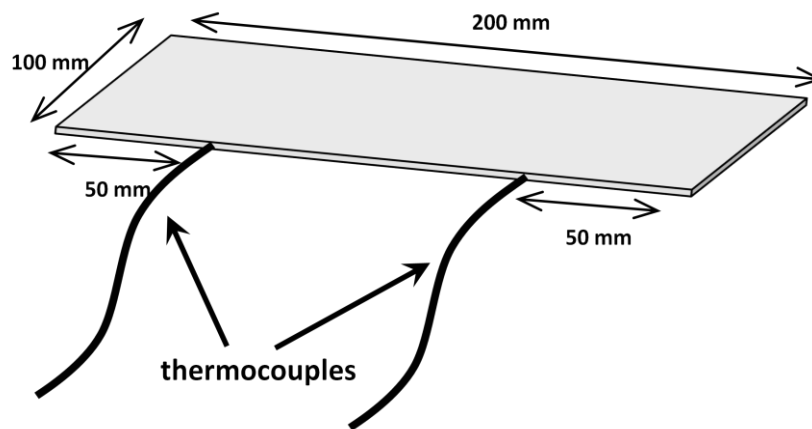


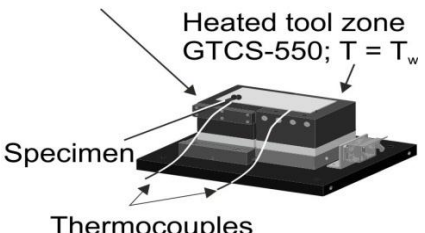
**Figure 11.** Specimen ready for being inserted into the furnace.

The position of the thermocouples were chosen aiming to measure a homogeneous temperature far enough from the edge of the specimen. This allowed the temperature to be calculated independently on each side of the specimen and determine the different temperature evolution under different temperature boundary conditions. The heated part of the tool was provided by 4 cartridges Z110 (630 W), this allowed the tool temperature to increase up to 500 °C.

As already done in former investigations regarding multiphase steel grades, the specimens were heated up to 850 °C and dwelled at this temperature for 4 minutes, in order to reach a homogeneous austenitic microstructure, Merklein & Svec (2012). At the same time, moderate austenitization temperature avoids excessive coating damage and met ecological and economical aspects, nowadays very important in the industry.

Afterwards, the austenitized specimens were transferred manually into the quenching tool and placed on adjustable spring-seated pins in order to avoid an early contact. Subsequently, the tool was closed using a hydraulic Lasco<sup>®</sup> TSPO100S press, which allows adjustable closing pressure. The entire route of transferring specimens to the press and the quenching was normally completed in 7÷8 seconds. Contact pressure and heated zone temperatures varied according to Table 3. The principal quenching tool layout is shown in the left side of Table 3.

**Table 3.** Tool and parameter settings for determination of the effect of the process parameters on the resulting material properties.

Quenching tool	Process parameters		
	Tool temperature [°C]		Contact pressure [MPa]
	heated	cooled	
	~ RT	RT	10
	400		20
500	40		
Press: Lasco TSP 100S0	Specimen dimension [mm] 100 x 200 x 1.75		
Control unit, measurement devices and electronic components			
Control unit:	HotSet Type HR06		
Heat cartridges:	Z110; 630 W; n=4		
Measuring board:	LKM101; cold junction: electronically by current		
Load cell:	Kistler 9091A; 1200kN		
Measurement amplifier:	ICAM 5073; ±10 V		
Transformer (temperature/force):	A/D; 16 bit		

The temperature profile was recorded by means of the thermocouples and, eventually, evaluated numerically according to equation (8). The ranges of temperature between which the HTC was valuated, was chosen in order to evaluate a constant cooling rate. The Table 4 shows the temperature actually chosen during the calculations.

**Table 4.** *Ranges of temperature actually chosen in dependency of the tool temperature.*

Water cooled tool temperature [°C]	Range of temperature [°C]	Heated tool temperature [°C]	Range of temperature [°C]
RT	700 ÷ 450	RT	700 ÷ 500
		400	750 ÷ 600
		500	750 ÷ 650

A minimum of three quenching tests were performed in each condition in order to guarantee repeatability. The time-temperature data profile was smoothed using a rolling average of 19 points.

Figure 12 depicts the facilities used during the press-hardening tests.





**Figure 12.** Facilities used during the press-hardening tests. Close-up, the Lasco<sup>®</sup> press is visible; the furnace is on the right side of the picture.

### 3.3 Micro-Hardness Tests

In order to characterize the developed microstructure after quenching, in dependency of used process parameters in the cooled and heated part of the tool, micro-hardness tests HV0.1 according to standard ISO 6507-1 (6507-1:2005) were performed.

For the microstructure characterization of the heated, cooled and transition zone, specimens from different parts of the processed blank were laser cut. Figure 13 shows the exact cutting position.

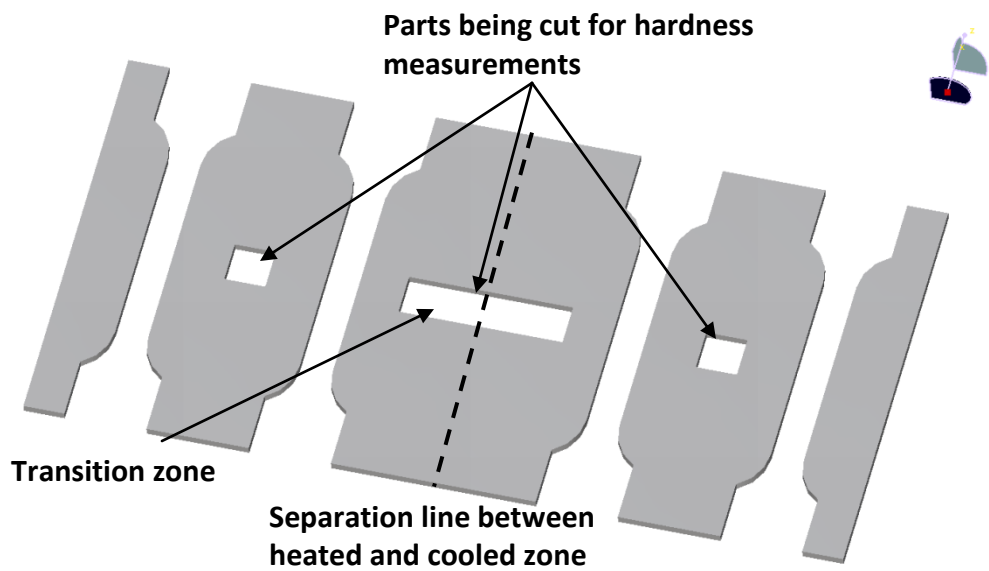


**Figure 13.** Parts being cut from the processed specimen in order to perform hardness measurement HV0.1.

The instrument used for the hardness measurements was a Fischerscope<sup>®</sup> HM200, equipped with WIN-HCU<sup>®</sup> software. The load of 0.9807 N was applied linearly from 0 N to 0.9807 N for 8 seconds and held constant at 0.9807 N for 10 seconds to compensate for elastic recovery effects. The distance between the measurement points along one line over the cross section was about 0.4 millimeters on the heated and cooled part; a distance

of 0.2 millimeters was used along the transition zone in order to appreciate the gradient of hardness due to the different boundary conditions applied.

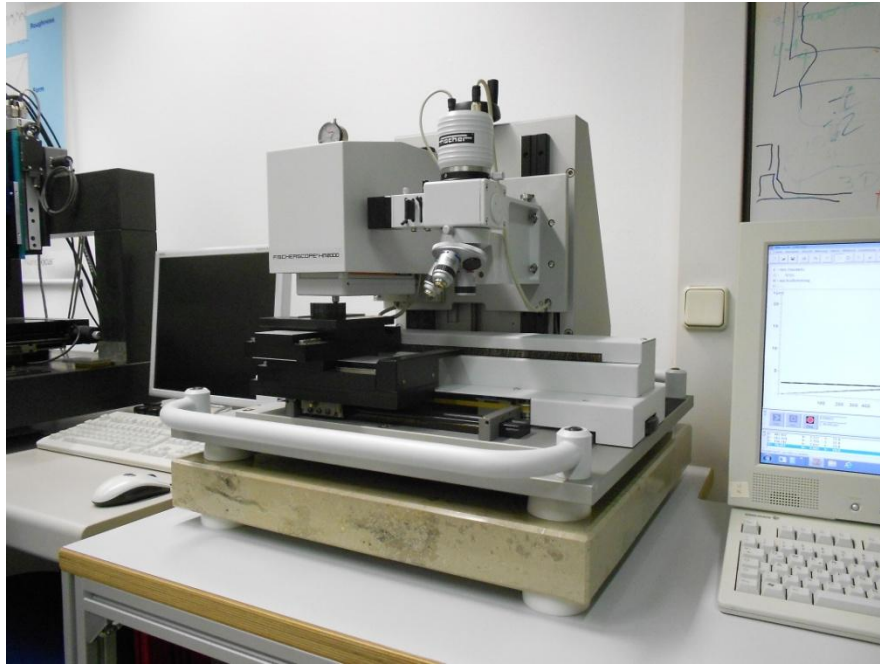


**Figure 14.** *Fischerscope<sup>®</sup> HM200 used to perform hardness measurements.*

### 3.4 Metallographic Analysis

In order to validate the measured hardness and to distinguish the different phases achieved in the steel consequently to the process formerly carried out, microstructure analyses by means of selective phase etching (Nital 3 %) and light optical microscope (LOM), provided by KEYENCE® VH-Z 500 lens and WIN-HCU software, were performed. The parts of the blank already embedded for the hardness measurement, were polished and etched in order to perform metallographic analyses, see Figure 15. LOM pictures were taken and magnifications of 500x and 2000x were chosen for both of the water cooled and the heated side as well as the transition zone.



**Figure 15.** *Embedments ready for metallographic analyses. The small ones are for heated and cooled side, the big ones are for the transition zone.*

### 3.4 Tensile Tests

In order to characterize the mechanical properties of the processed material under pressure and temperature variations, tensile tests, according to standard ISO 6892-1 (6892-1:2009) were carried out. Specimens with a gauge length of 48 millimeters were cut from the previously press-hardened blanks. The detailed measures of the specimens are showed in Figure 16.

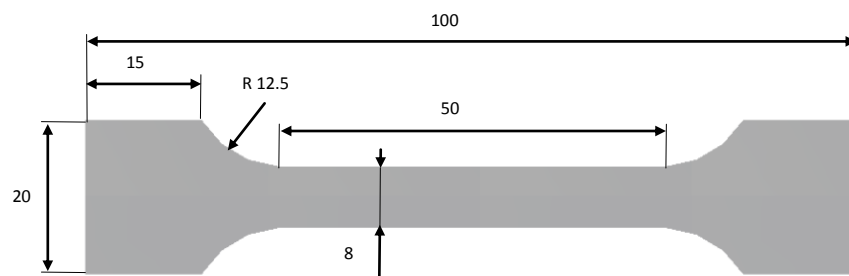


**Figure 16.** Dimension of the specimen used for tensile tests.

The facility used during the tests was an electro-mechanical tensile machine, Zwick/Roell<sup>®</sup> ZMART.PRO, depicted in Figure 17, equipped with the testXpert<sup>®</sup> II software.



**Figure 17.** *Tensile test machine Zwick/Roell<sup>®</sup> ZMART.PRO and CCD camera.*

The strain was measured by means of the optical strain measurement system ARAMIS<sup>®</sup> coupled to a GOM<sup>®</sup> CCD camera, Figure 17. The frame rate was varied from 4 to 6 Hz, in accordance with the specimen analyzed. Before the tensile test, the specimens were cleaned and painted using a white background and a graphite stochastic pattern. Parameters regarding the mechanical properties were calculated, such as yield strength, ultimate tensile strength, and elongation. The discussion is in the next chapter.

The Figure 18 shows in a) the stochastic pattern applied on the specimen just before fracture, and b) shows the corresponding major strain distribution detected by means of the ARAMIS<sup>®</sup> system.

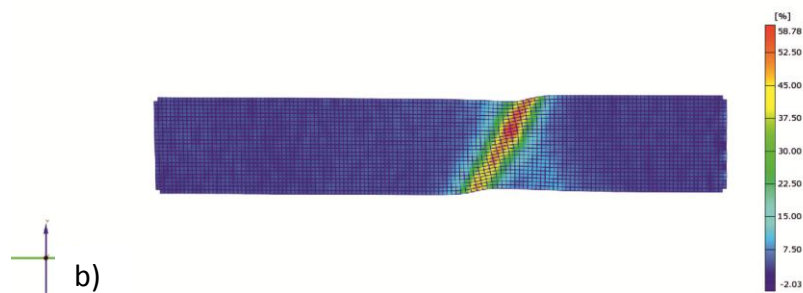
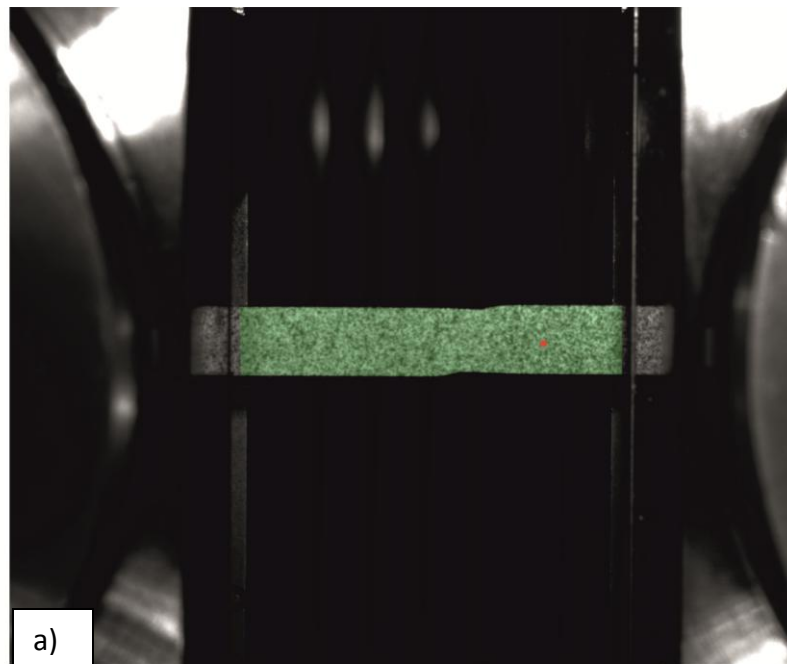


**Figure 18.** a) stochastic pattern of a specimen during a tensile test; b) major strain calculated by means of the ARAMIS<sup>®</sup> system





# Results

### 4.1 Influence of Process Parameters on Heat Transfer

As already mentioned in the previous chapters, many parameters might influence the resulting heat transfer coefficient (HTC) between the blank and the tool while quenching occurs. Accordingly to equation (9), the dissimilar difference of temperature between the specimen and the tool, in the heated and cooled zone, influences the cooling rate and consequently the mechanical properties of the processed steel. Additionally, higher applied contact pressure might enhance the HTC by smoothing of the asperities between the tool and specimen contact surface.

Concerning the DP-K 45/78 steel grade, a substantial different behavior could be noted if compared to the complex phase steel. No influence of the applied pressure is visible in the room temperature and 400 °C tests, in which the HTC in the heated tool zone is around  $5 \text{ kW}\cdot\text{m}^{-2}\cdot\text{K}^{-1}$ ; in the cooled zone ranges from around  $6.3 \text{ kW}\cdot\text{m}^{-2}\cdot\text{K}^{-1}$  to more than  $7 \text{ kW}\cdot\text{m}^{-2}\cdot\text{K}^{-1}$  respectively for the room temperature and the 400 °C tests. By contrast, the pressure has a remarkable influence in the 500 °C tests for both sides of the tool. In this case the HTC gains from  $6 \text{ kW}\cdot\text{m}^{-2}\cdot\text{K}^{-1}$  to  $9.5 \text{ kW}\cdot\text{m}^{-2}\cdot\text{K}^{-1}$  in the water cooled side and from  $3 \text{ kW}\cdot\text{m}^{-2}\cdot\text{K}^{-1}$  to  $5.1 \text{ kW}\cdot\text{m}^{-2}\cdot\text{K}^{-1}$  in the heated tool zone. In all cases, the different tool steel properties between heated and cooled zone, strongly influences the

resulting HTC, which is appreciably lower for the tool steel GTCS-550 in all the cases analyzed.

Regarding the steel grade CP-W 800, tests with heating cartridges off show a noticeable increase of the HTC with applied pressure, for both sides of the tool; the cooled side varies in a range between  $4.7 \text{ kW}\cdot\text{m}^{-2}\cdot\text{K}^{-1}$  and  $7.1 \text{ kW}\cdot\text{m}^{-2}\cdot\text{K}^{-1}$  and the heated side varies between  $3.1 \text{ kW}\cdot\text{m}^{-2}\cdot\text{K}^{-1}$  and  $4.8 \text{ kW}\cdot\text{m}^{-2}\cdot\text{K}^{-1}$  respectively for 10 MPa and 40 MPa. On the other hand, no influence of applied pressure is observable concerning tests carried out with heat cartridges on. Moreover, the increase of temperature in the heated tool does not result in appreciable influence of the HTC of the heated part itself, resulting in a quite uniform HTC around  $4 \text{ kW}\cdot\text{m}^{-2}\cdot\text{K}^{-1}$ , slightly increasing to  $4.6 \text{ kW}\cdot\text{m}^{-2}\cdot\text{K}^{-1}$  at 40 MPa and 500 °C. The enhanced tool temperature, rather, influences the HTC of the cooled side, showing a strong enhancement from around  $6 \text{ kW}\cdot\text{m}^{-2}\cdot\text{K}^{-1}$  to  $8 \text{ kW}\cdot\text{m}^{-2}\cdot\text{K}^{-1}$ . In all cases, the different tool steel properties between heated and cooled zone, strongly influence the resulting HTC, which is appreciably lower for the tool steel GTCS-550 in all the cases analyzed.

Comparing the HTC behavior between complex phase and dual phase steel grades, a substantial difference can be noted, namely that the complex phase shows HTC pressure dependency during room temperature tests while the dual phase steel grade shows a great pressure dependency only during the 500 °C tests. By contrast, the dual phase HTC between 20 MPa and 40 MPa at 500 °C, in the heated side of the tool, has only a slight enhancement of less than 12 %.

Figure 19 displays the average of three calculated heat transfer coefficients between the contact surfaces of the heated and cooled tool zone and the specimen, for both the steel grades object of the study. On the bottom of the figure are depicted exemplary cooling-curves with both part of the tool at room temperature; the discrepancy between the heated and cooled zone is due to the different tool steel properties and the lack of active water cooling in the heated part.

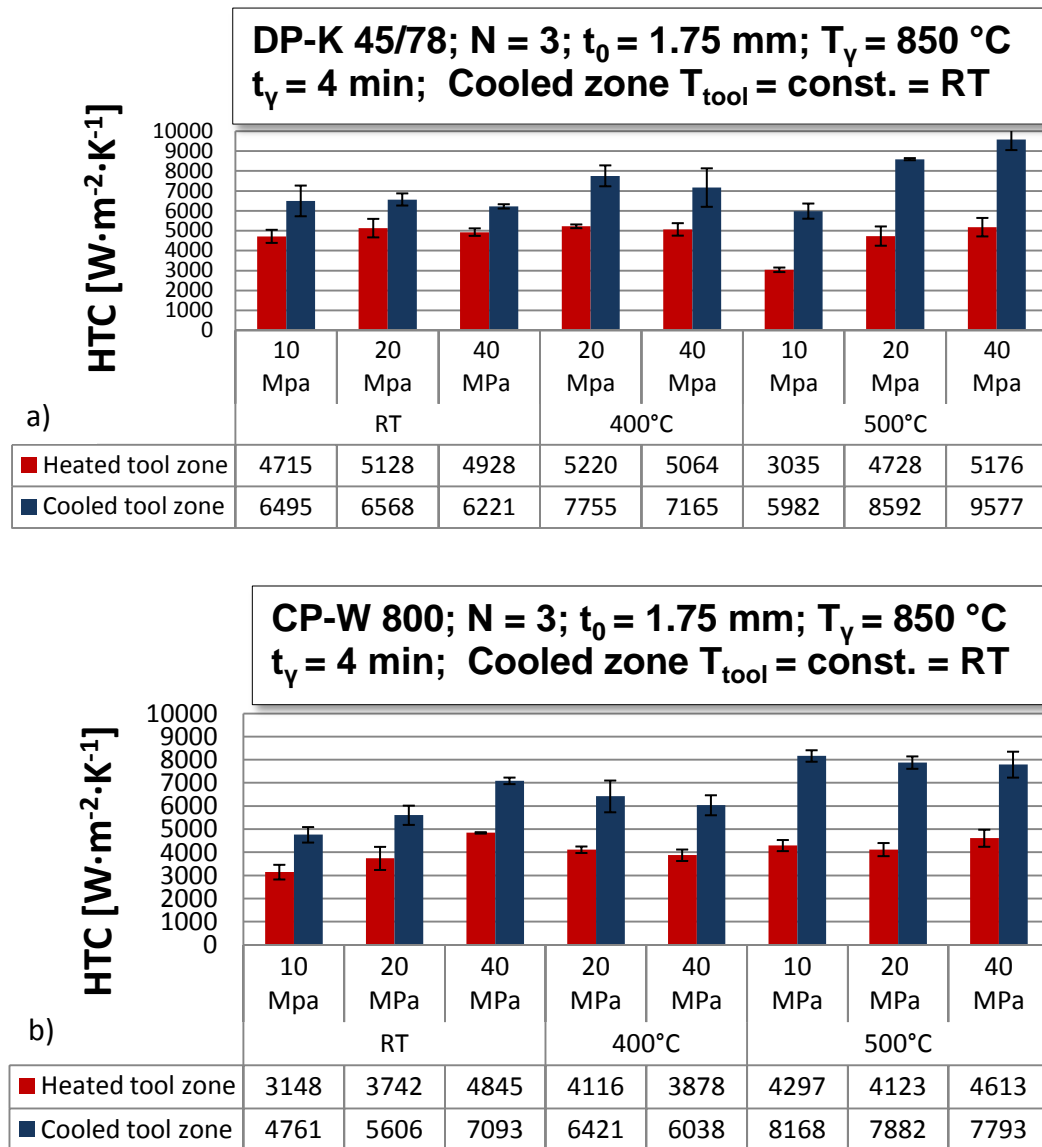


**Figure 19.** Heat transfer coefficient calculated experimentally. a) Dual phase steel; b) complex phase steel.

In order to better understand the temperature-pressure dependency of the heat transfer coefficient, the thermal characteristics are plotted as a function of the blank's temperature. In Figure 20 and Figure 21 is depicted the heat transfer coefficient as a function of the blank temperature in dependency of the applied pressure and tool temperature for both the steel grades investigated during the present study. It can be noted the accordance to

the HTC values calculated in Figure 19, namely a visible pressure dependency is shown in the tests with heated tool at 500 °C for the dual phase steel grade and for the room temperature tests for the complex phase steel grade.

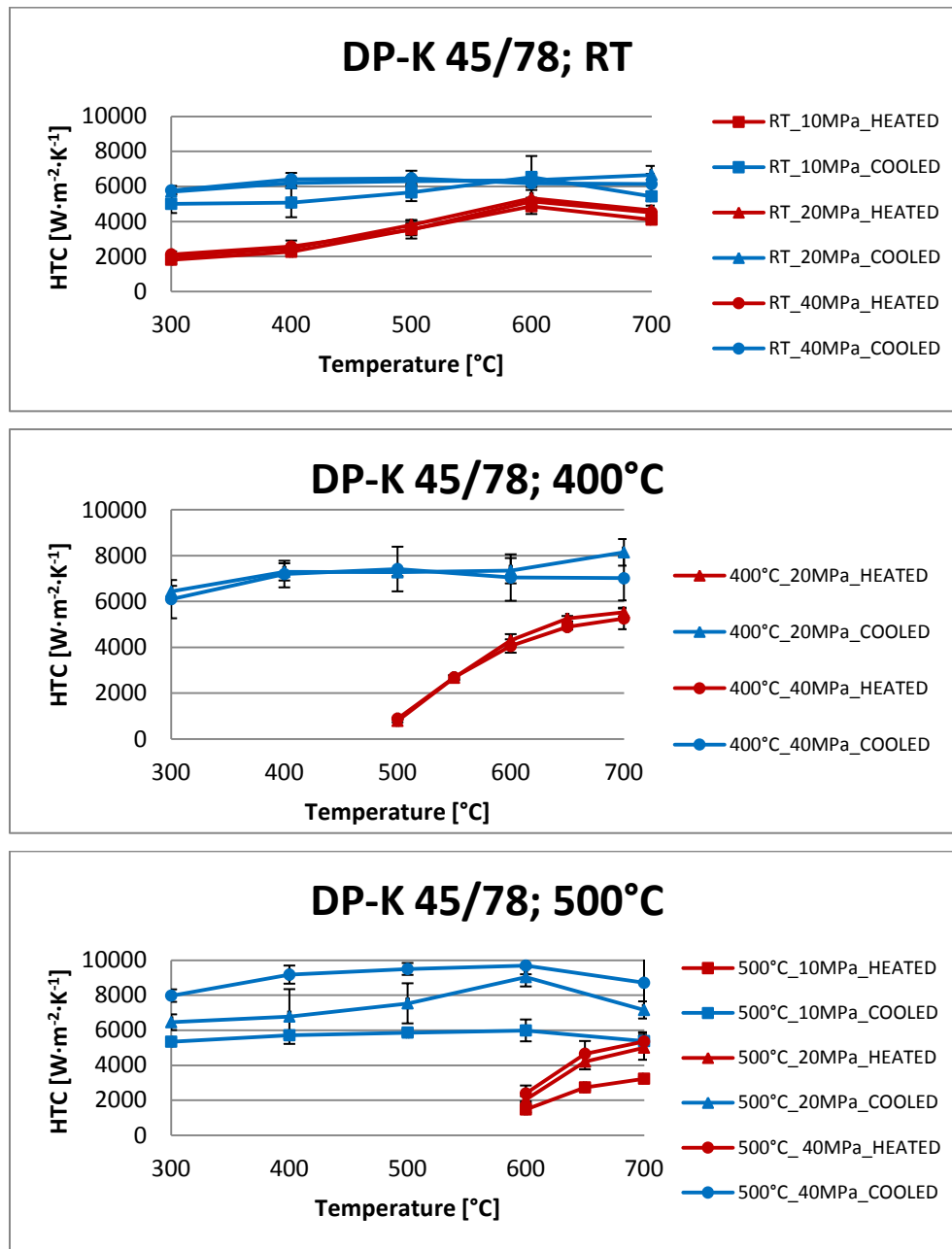


**Figure 20.** Heat transfer coefficient between the dual phase specimen and tool as a function of the temperature of the blank in dependency of the tool temperature and contact pressure. From the top to the bottom, tests with heated tool at room temperature, 400 °C and 500 °C are depicted.

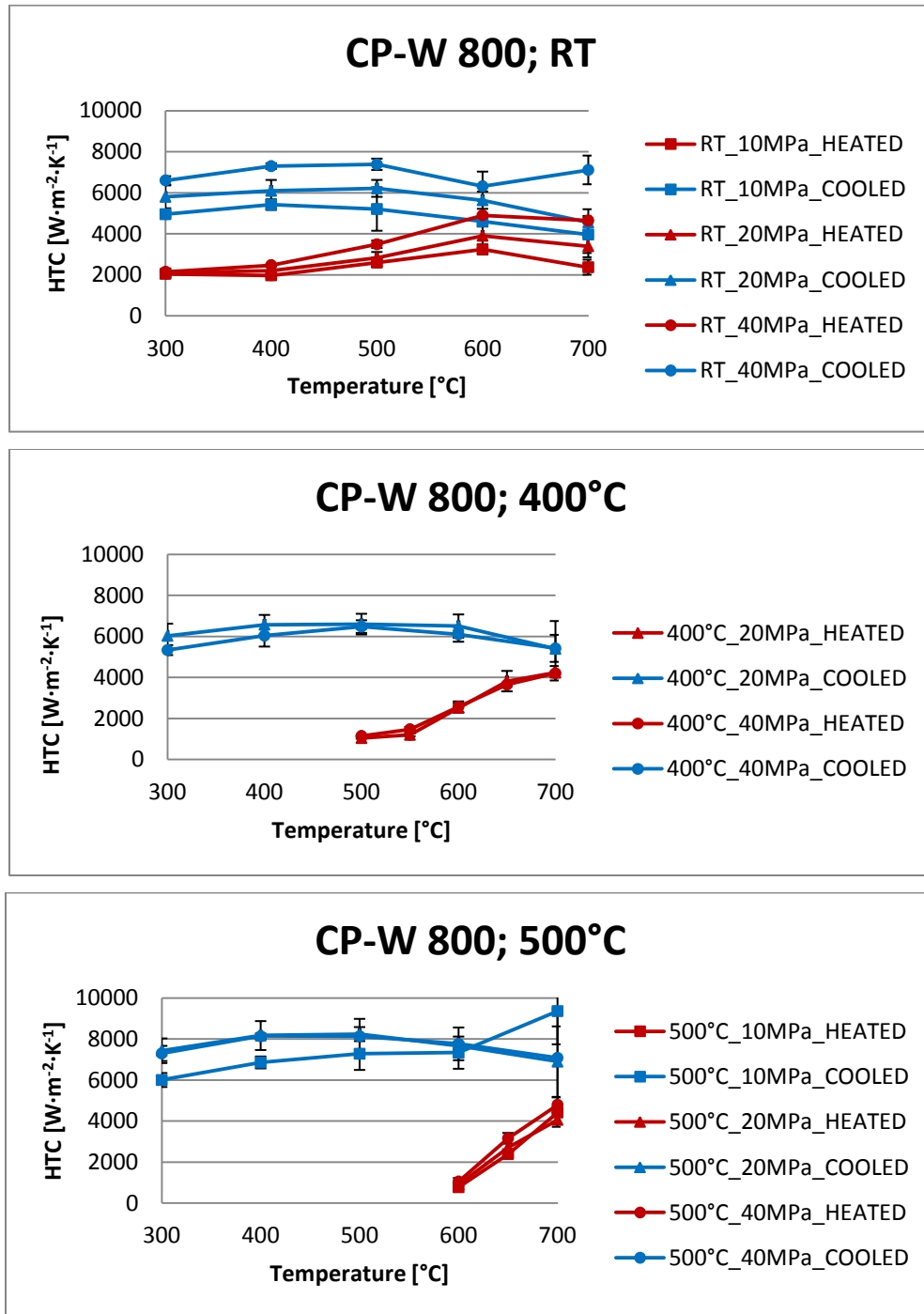


**Figure 21.** Heat transfer coefficient between the complex phase specimen and tool as a function of the temperature of the blank in dependency of the tool temperature and contact pressure. From the top to the bottom, tests with heated tool at room temperature, 400 °C and 500 °C are depicted.

## **4.2 Characterization of the Developed Microstructure**

The resulting microstructures are characterized firstly by hardness measurements HV0.1 according to the standard ISO 6507-1 and, subsequently, by metallographic analysis, performed by etching 3 % Nital and LOM images. In this chapter the hardness measurements results are described; in the next chapter, the metallography results will be revealed.

Concerning the dual phase steel, looking at Figure 22 (a), it can be noted that there is no significant impact of the adjusted temperature on the heated part of the tool on the measured hardness of the cooled part of the specimen, which exhibits a value slightly above 480 HV0.1, a characteristic value for a mainly martensitic microstructure. Similarly, the heated part of the specimen shows no dependence on applied contact pressure. The heated part of the tool, with cartridges off, displays a nonsignificant decrease of the micro-hardness compared to the water cooled side, leading to the assumption of a modest difference in the resulting microstructure. By contrast, great impact on the resulting hardness appears when the cartridges are on, precisely, when the heated tool is at 400 °C, the measured micro-hardness is almost 290 HV0.1. A further hardness values abatement is achieved at 500 °C, leading to a value around 250 HV0.1. These are both typical values for softer mixed ferritic-pearlitic-residual austenitic microstructure.

The micro-hardness analyses carried out on the complex phase steel grades show comparable behavior to the dual phase steel grade but with somewhat lower values, see Figure 22 (b). All the tests show no hardness dependency on the contact pressure. Moreover, the measurements performed on the water cooled side display micro-hardness values around 430 HV0.1; slightly lower values appear for heated side with cartridges off, namely 405 HV0.1. These values let the assumption be made of a mainly martensitic metallographic composition. By increasing tool temperature to 400 °C, hardness on the heated side drops to about 250 °C; a slightly lower hardness value of 220 °C is achieved setting the heated part of the tool up to 500 °C. These values lead one to assume a soft mixed microstructure composed of ferrite, pearlite and residual austenite.

The comparison between the two steel grades as object of the study shows an overall greater hardness value for all the tests carried out on the dual phase. This means a better temperability for this steel grade, confirmed by the higher carbon content. At the same time, a higher carbon content might negatively affect the weldability. For these reasons each one of the steels analyzed might be suitable for different applications.



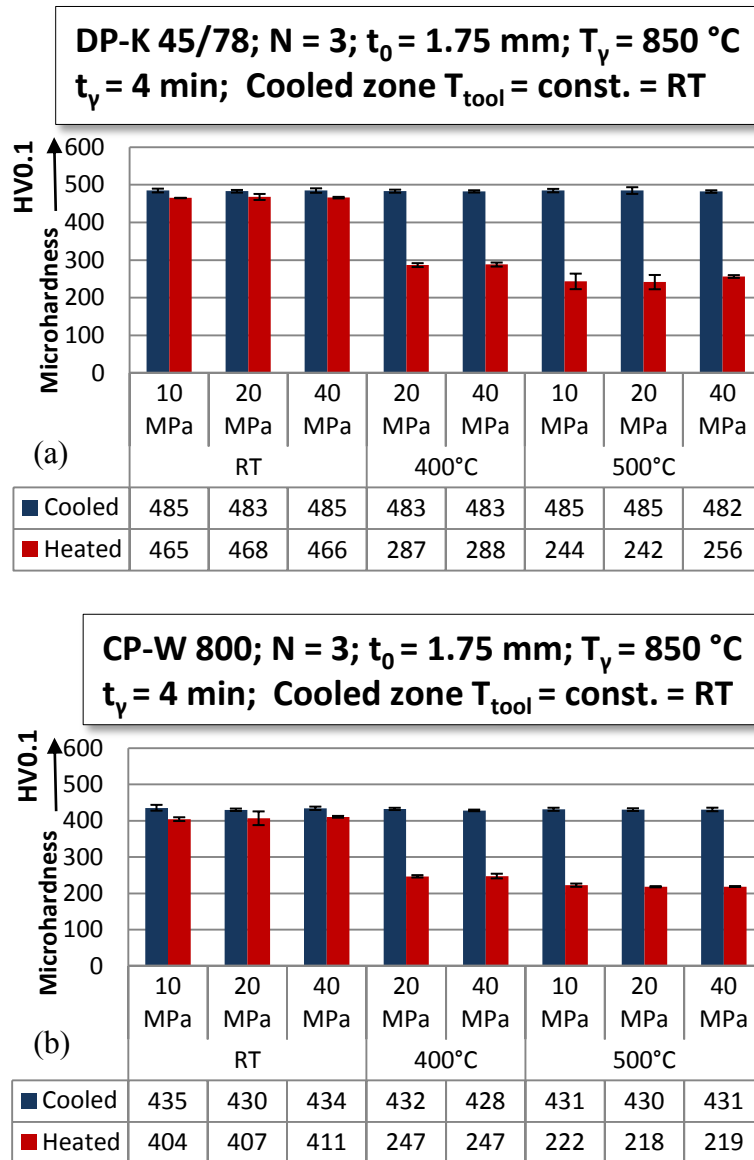


**Figure 22.** Results of hardness tests HV0.1.(a) dual phase results; (b) dual phase results.

In the literature, values regarding the boron-manganese 22MnB5 steel grade are easily available, Svec & Merklein (2011), showing a lower tool-temperature response for this steel. Namely, a very soft structure (240 HV0.1) is achieved with heated tool temperature

at 500 °C, while a tool temperature of 400 °C shows hardness values of more than 400 HV0.1, typical of a mainly bainitic microstructure. Since there is a great amount of power necessary to heat up quenching tools, these results lead one to assume a better energy efficiency is possible in an industry process by increasing temperature in certain zone of the tool when using multiphase steels in order to achieve adjusted material properties in a unique sheet metal

Further hardness measurements have been carried out on the transition zone of the specimen, in order to figure out its crucial features.

As expected for both the steel grades under investigation, no visible hardness alteration appears along the transition zone, Figure 23, when the heated part of the tool is at room temperature; moreover no pressure dependency is observable. As previously mentioned, remarkable changes occur when the heated tool is at 400 °C and 500 °C. Regarding the dual phase steel, hardness starts to decrease to around  $x = 18$  millimeters, i.e. very close to the separation line between the two tool steel grades. Moreover, the hardness gradient extends more than 22 millimeters, namely beyond the graph end. For this reason, in order to figure out the actual length of the hardness gradient, an extended measurement length would be necessary.

By contrast, considering the complex phase steel grade, the hardness gradient starts around the coordinate  $x = 13$  millimeters, visibly before that of the dual phase steel grade. In this case, the hardness gradient extension is narrower, around 17 millimeters. This difference might be attribute to different heat conductivity between the two materials.

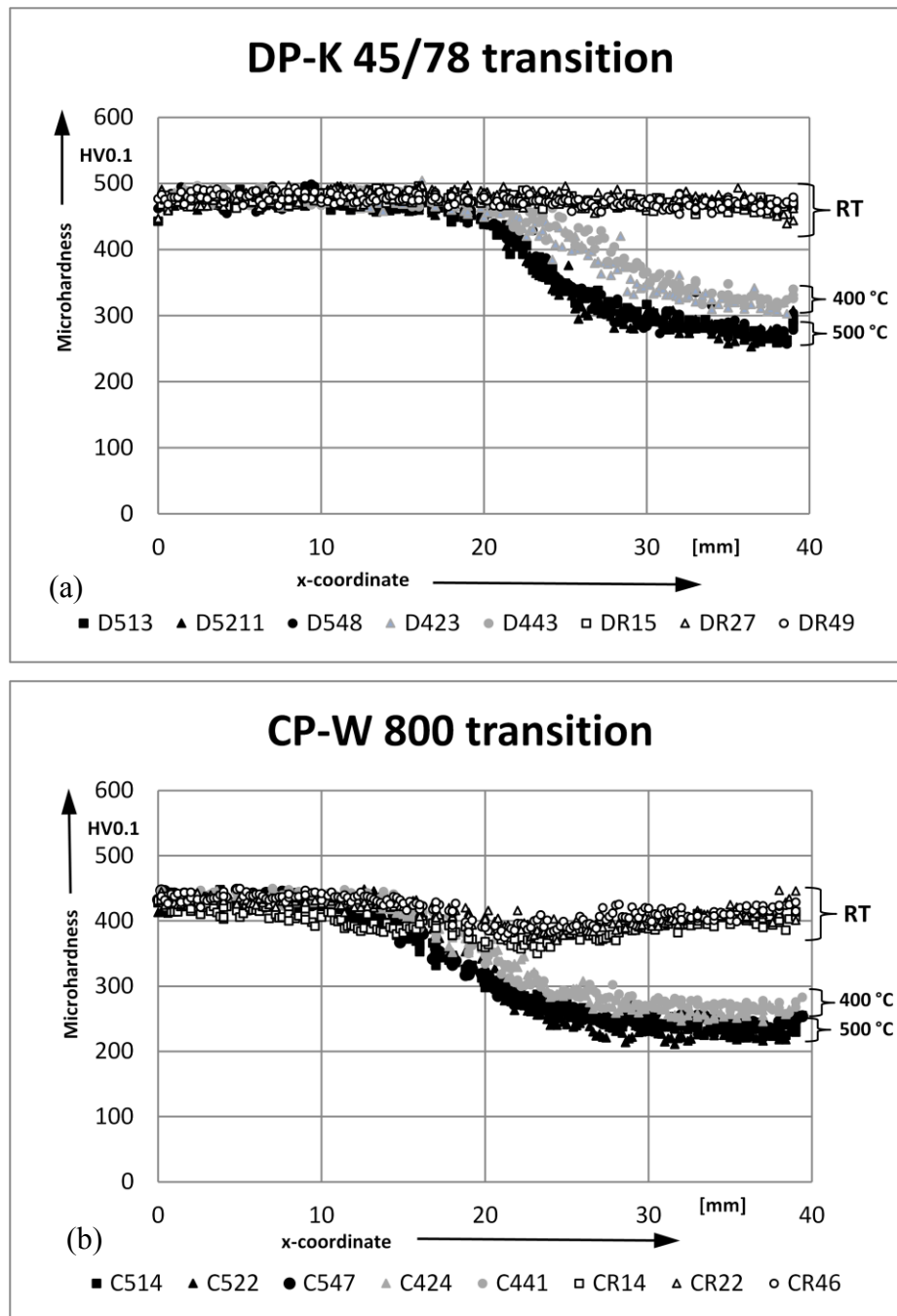
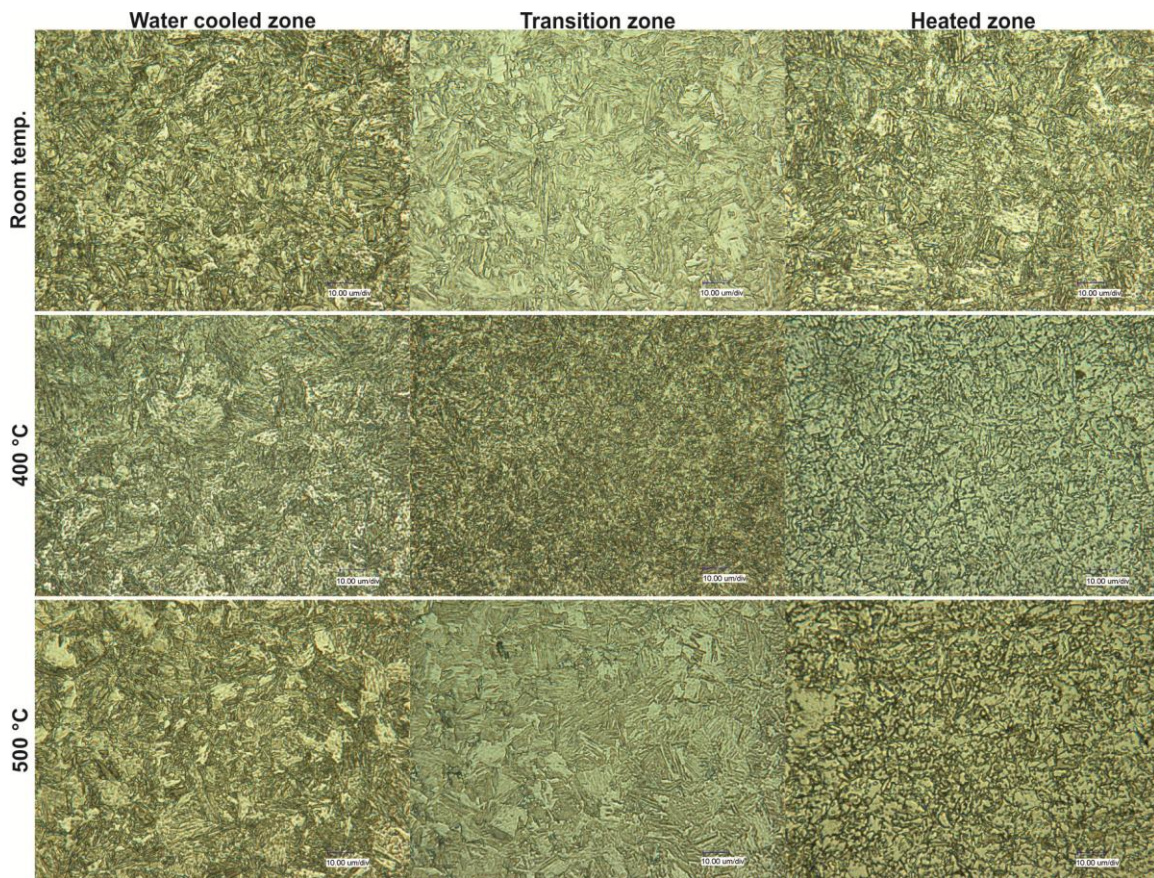


**Figure 23.** Characterization of the transition zone between heated and cooled part by hardness measurements on the specimen. (a) dual phase steel; (b) complex phase steel.

### 4.3 Metallographic Analyses

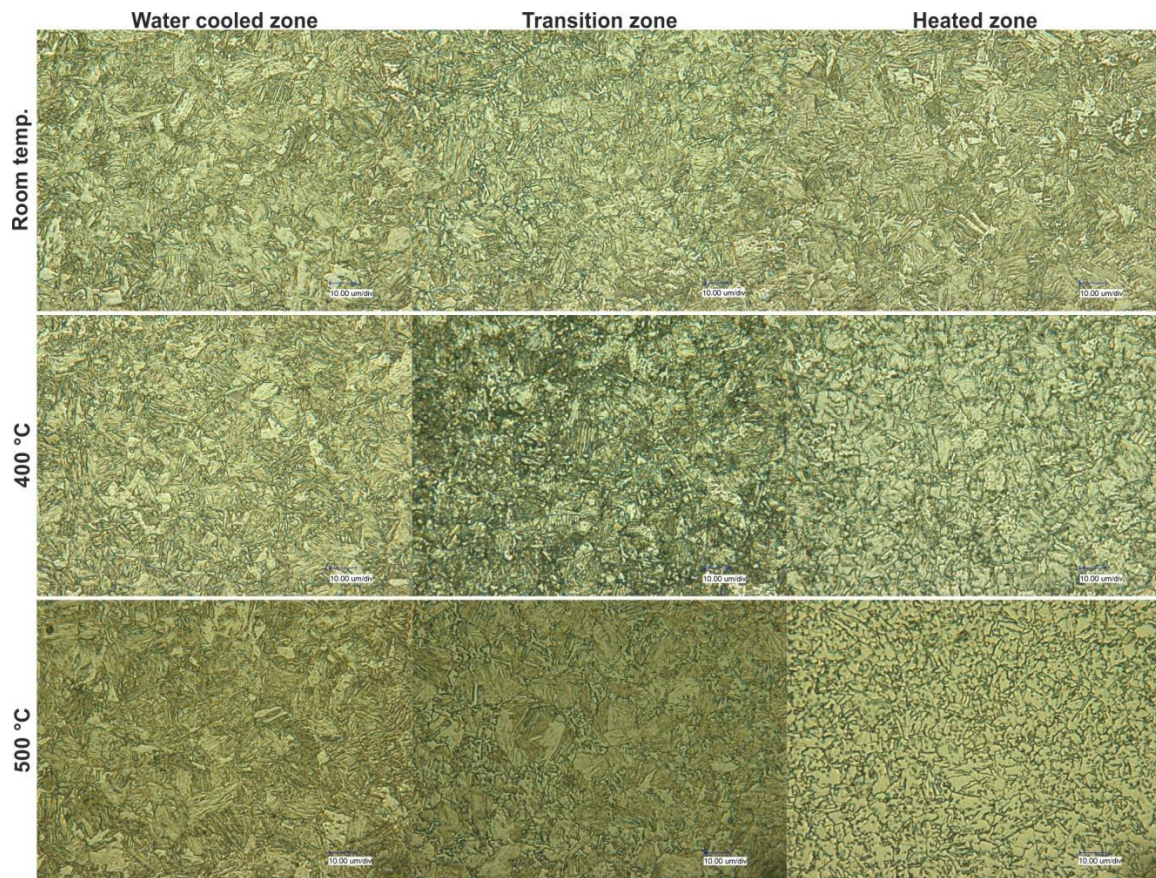
In this paragraph, the assessed microstructure by hardness measurement is going to be confirmed by metallographic analyses, carried out by means of etching 3 % Nital and LOM images.

Figure 24 and Figure 25 display exemplarily the microstructure of the specimens in dependency of tool temperature in the heated part of the tool and applied contact pressure of 20 MPa. Irrespective of the adjusted tool temperature in the heated part of the tool, a lath martensitic microstructure developed in the cooled side of the specimen. Furthermore, martensitic microstructure is present also in the heated part of the tool at room temperature. Thus, no visible microstructure modifications occur when the tool steel GTCS-550 is used. On the other hand, remarkable changes of microstructure occur in tests with heated tool at 400 °C and 500 °C. In these cases a mostly globular ferritic microstructure is developed. Concerning the transition zone with heated side at 400 °C and 500 °C, a distinction should be done between the dual phase and the complex phase steel grades, the first one shows a mostly martensitic microstructure, very similar to the water cooled side, and the second one displays a mixed microstructure, with less amount of martensite. The results are in accordance with the gradient of microhardness presented in the former paragraph.



**Figure 24.** Metallographic analyzes of the developed microstructure in the cooled and heated zone as well as in the transition zone of the dual phase steel, in dependency of tool temperature shown exemplarily for  $p_c = 20$  MPa. Magnification 2000x. LOM images.





**Figure 25.** . Metallographic analyzes of the developed microstructure in the cooled and heated zone as well as in the transition zone of the complex phase steel, in dependency of tool temperature shown exemplarily for  $p_c = 20$  MPa. Magnification 2000x. LOM images.

In addition, referring to the CCT diagrams presented in the studies carried out by the Authors Neugebauer *et al.* (2011), the slight increase of hardness in the heated part at 400 °C compared to the one at 500 °C might be ascribed to a more significant amount of phases like pearlite and bainite, together with the ferritic matrix.

#### **4.4 Evaluation of Mechanical Properties**

In this paragraph, the main mechanical properties, in dependency of applied pressure, tool temperature and material, have been investigated by means of tensile tests in accordance to standard ISO 6892-1.

Regarding the dual phase steel grade, see Figure 26, mechanical properties such as ultimate tensile strength (UTS), yield strength (YS), ultimate elongation at fracture (UTE) and uniform elongation (UE) are not influenced either by pressure or by temperature in the heated part of the tool; UTS values are around 1400 MPa, YS are around 1000 MPa, UTE are around 8 % and UE around 4 %. In addition, the GTCS-550 tool steel at room temperature does not influence significantly these properties since the mechanical properties remain almost the same. First noteworthy changes in the mechanical properties occur when the cartridges are on and, consequently, the heated part of the tool is first at 400 °C and then at 500 °C. When the heated part of the tool is at 400 °C, the UTS drops to around 800 MPa and the YS to around 600 MPa; the UTE increases remarkably to 14 % and, at the same time, YE increases to 8 %. Increasing the heated tool temperature up to 500 °C on one hand creates no visible differences in UTS values in comparison to the 400 °C test, and on the other hand causes YS to decrease to 480 MPa and both UTE and UE increase to 19 % and 14 % respectively.

Concerning the complex phase steel, see Figure 27, no influence of the applied pressure is detected; additionally, no influence of the heated tool temperature appears in the water cooled side of the specimen in which UTS and YS values around 1200 MPa and 950 Mpa and UTE and UE values around 8 % and 4 % are respectively exhibited. When compared to the water cooled side, the GTCS-550 tool steel at room temperature slightly influences the UTS and YS, which are around 1130 MPa and 870 Mpa respectively, but UTE and UE are not affected. Similar to dual phase steel, the complex phase shows great temperature dependency when the tool is heated up to 400 °C and 500 °C. The UTS and YS drop to 700 MPa and 580 MPa respectively, and the UTE and YE increase to 17 % and 9 %. In addition, the tool temperature at 500 °C leads to a further reduction of

strength; namely, values around 660 MPa and 440 MPa for UTS and YS are exhibited. The elongation increases remarkably, i.e. 22 % and 15 % for UTE and UE respectively. Comparing the dual phase steel to the complex phase one, it can be noted the first one has greater strength during all the comparable tests conditions investigated. By contrast, the elongation remains at the same value in the water cooled side of the specimen irrespective of the steel grade being examined. Moreover, when the heated part of the tool is at a high temperature, the complex phase steel shows lower strength but exceptional elongation (UTE up to 22 % when the tool temperature is 500 °C).

Considering the study carried out by the Authors Merklein & Svec (2013), a basic comparison between the multiphase steels investigated in the present work and the 22MnB5 can be made. The boron-manganese steel grade exhibits an extraordinary temperability, gaining a UTS up to 1500 MPa and UTE of about 6 % using water cooling. UTS around 700 MPa and UTE beyond 15 % were achieved when a heated tool at 500 °C was employed, bringing these values very close to the dual phase ones. The complex phase steel shows lower strength when quenched using a water cooled tool but, with a heated tool at 400 °C, presents comparable properties to the 22MnB5 using a 500 °C tool, and leading to possible savings of power, and therefore of money, for heating up the quenching apparatus. Using a tool temperature of 500 °C for quenching the complex phase steel, even better elongation is achieved, leading to the supposition of good suitability for energy-absorbing parts in the body in white.



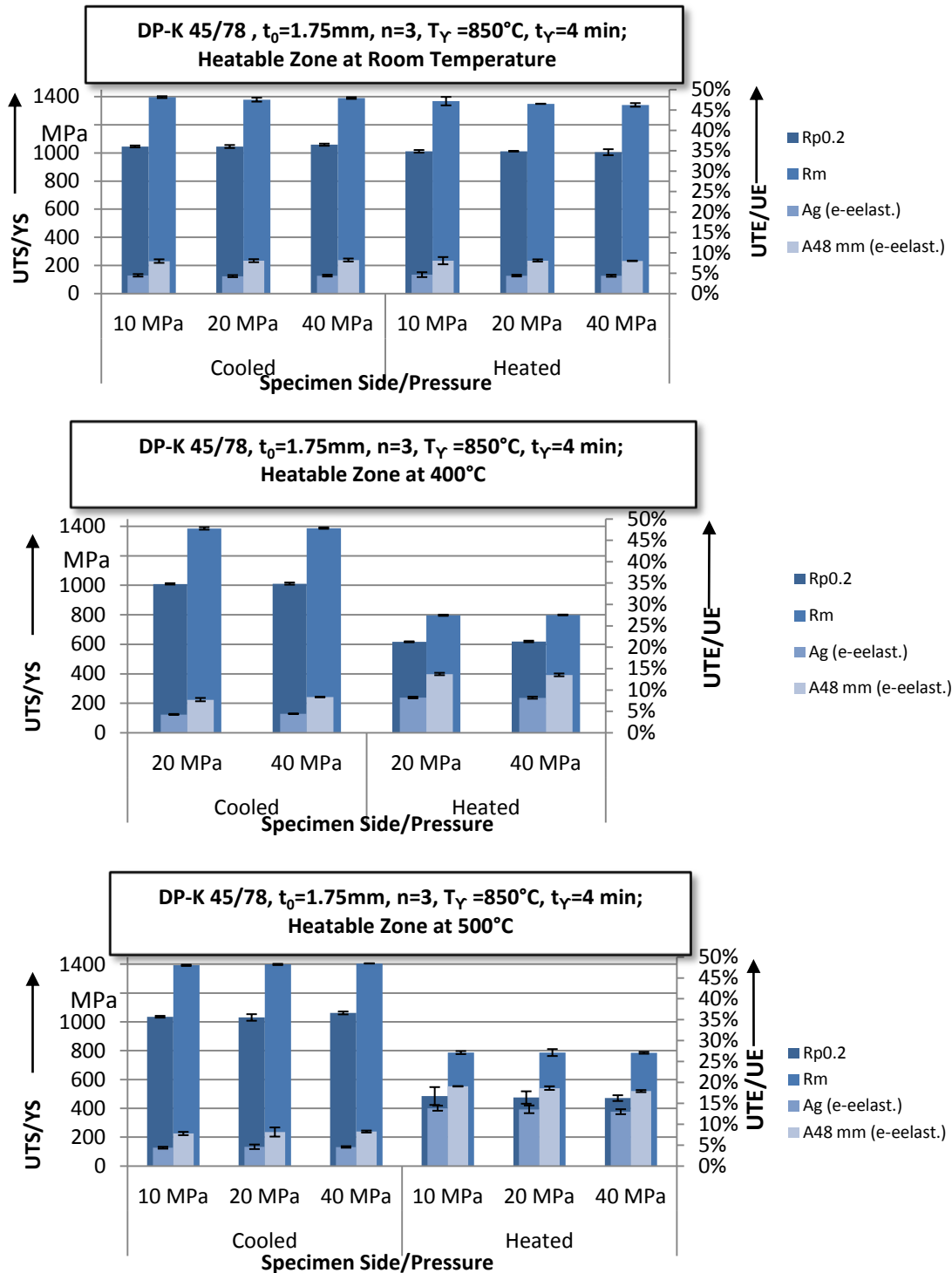


Figure 26. Mechanical properties of the dual phase steel grade investigated in the present study.

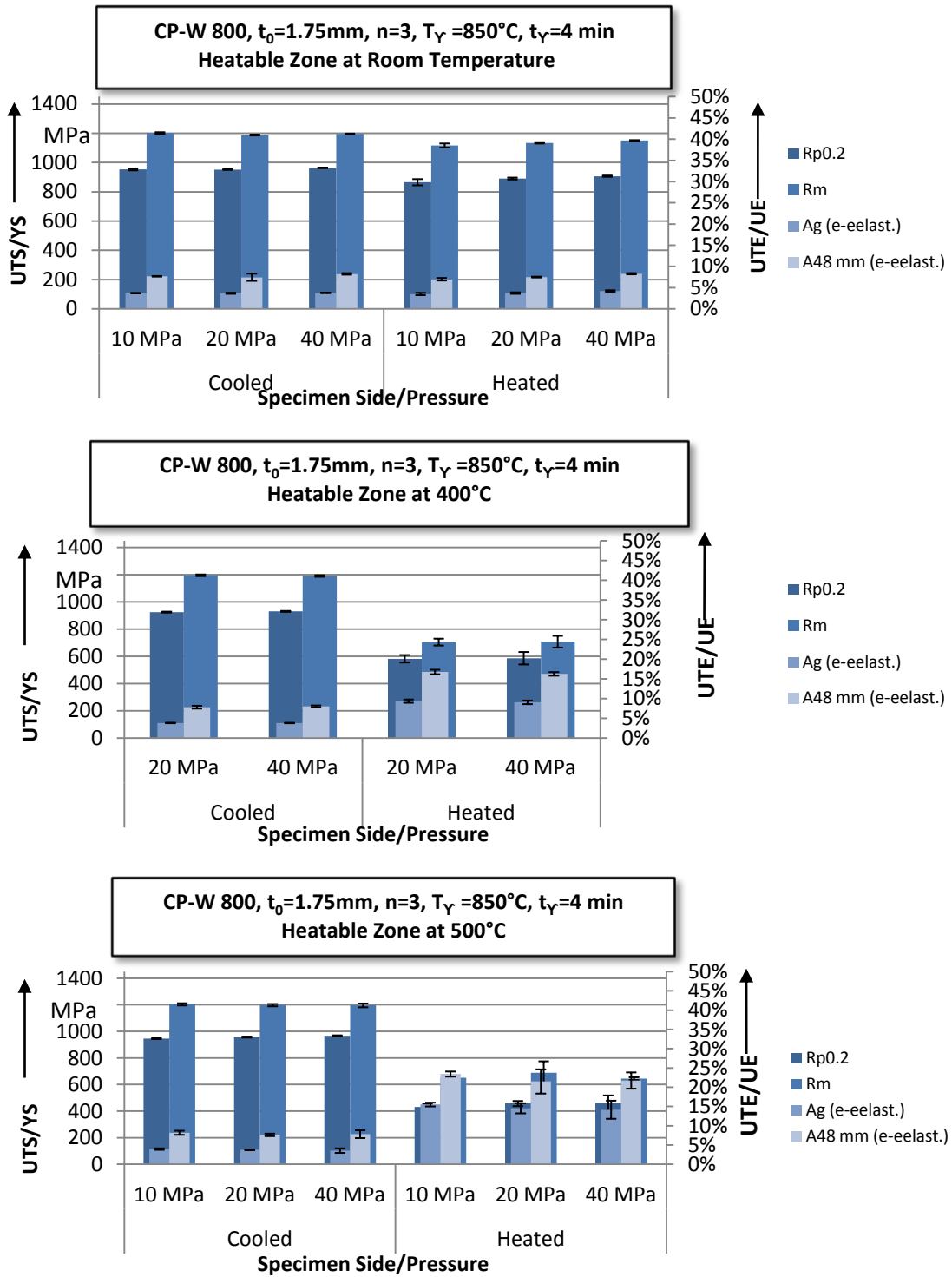
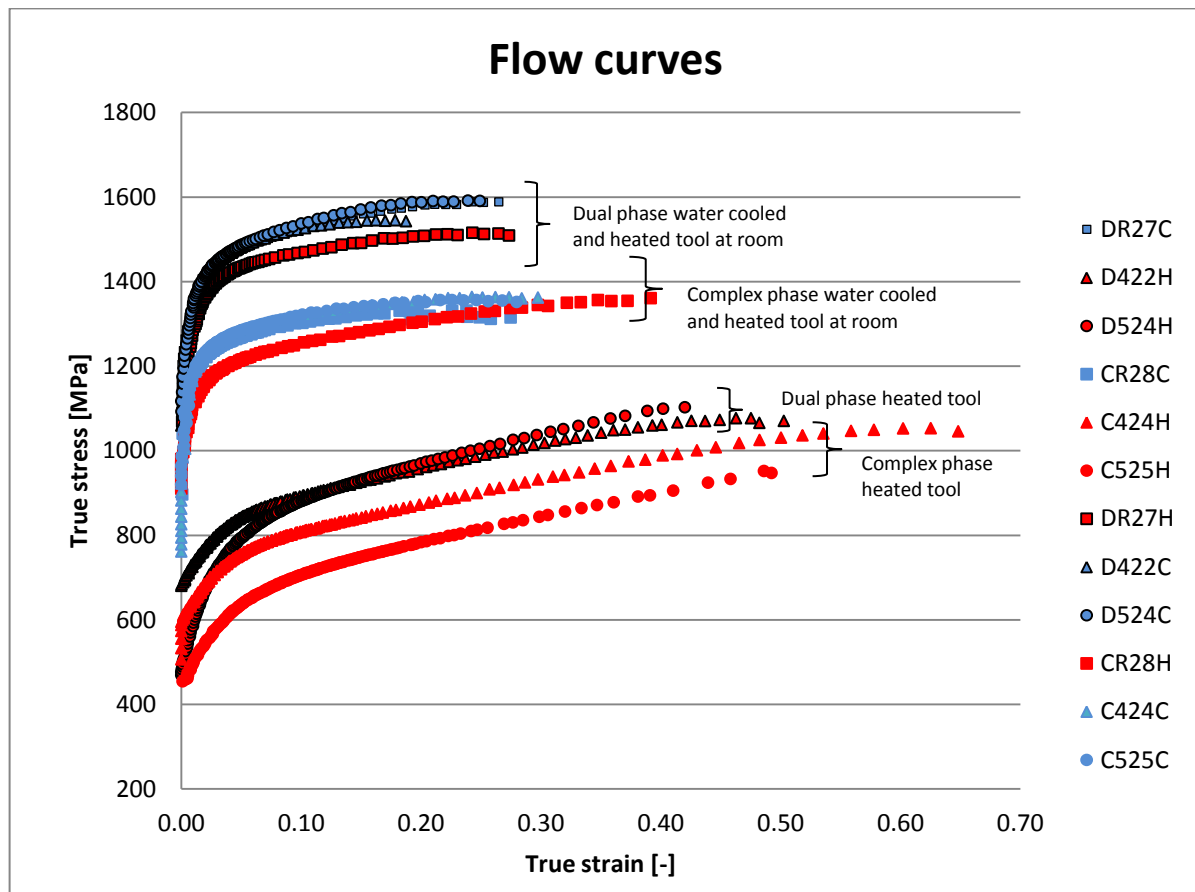


Figure 27. Mechanical properties of the complex phase steel grade investigated in the present study.

Figure 28 displays exemplary flow curves for quenching tests carried out at 20 MPa. It can be noticed that the flow curves are consistent with mechanical properties formerly discussed. It can be clearly seen that the dual phase, quenched with a water cooled tool, has the greatest strength and that the GTCS-550 tool steel at room temperature has a rather small impact on the flow curves of both the steel grades. The lowest stress and the highest strain is reasonably exhibited by the complex phase steel quenched with the high temperature tool.

**Table 5.** Flow curve's legend of Figure 28.

Heated zone temperature [°C]	Dual phase		Complex phase	
	Heated	Cooled	Heated	Cooled
RT	■	■	■	■
400	▲	▲	▲	▲
500	●	●	●	●



**Figure 28.** Exemplary flow curves at 20 MPa showing the behavior of the dual phase and complex phase steel under different temperature conditions.

# Outlook

## 5.1 Outlook

Hot forming is nowadays a well-established process in automotive industry which allows the manufacturing of ultra-high strength components in order to save weight and, at the same time, improve crashworthiness.

The breakthrough process in hot forming, the so-called tailored tempering, allows to achieve locally adjusted properties in a unique hot formed part in order to meet the even increasingly stricter safety requirements and maintain accordance with light-weight design standards.

The common high-strength steel for hot stamping processes is the boron-manganese 22MnB5 steel grade, which results in up to 1500 MPa tensile strength and almost 6 % ultimate elongation, after being processed. Recently, a tailored approach has been studied, leading, to a UTS close to 700 MPa and a ultimate elongation of more than 15 % when a heated tool is used.

The main objective of the present research was to characterize, in absence of deformation, multi-phase steel grades, such as the DP-K 45/78 and the CP-W 800, marketed by ThyssenKrupp, varying process relevant conditions, such as tool temperature and contact pressure.

Results showed that the heat transfer coefficient is not always affected by the applied contact pressure. By contrast the different tool steel being used influences the heat transfer coefficient considerably. Moreover, it was proven that the maximum UTS achievable for the dual phase steel and the complex phase is 1400 MPa and 1200 MPa respectively. When the tool is heated up to 400 °C, the complex phase steel shows an interesting ultimate elongation of about 17 % and a remarkable 22 % when the tool is at 500 °C. Both the steel grades investigated have a better response to the tailored properties at 400 °C, if compared to the 22MnB5 steel grade. Moreover, it would be interesting to investigate the response to 300 °C tool temperature, in order to obtain, if possible, a more economical process.

Since the present research was an investigation carried out in order to find out the dependency on main process parameters typical of the industrial hot forming processes but in absence of deformation, further studies are necessary to understand the deformation influence on multi-phase steels. In addition, a finite element simulation would be necessary to verify the applicability of the HTC calculated experimentally.

## References

- 6507-1:2005, International Standard.  
6892-1:2009, International Standard.
- Åkeström, P. (2006). *Modelling and Simulation of Hot Stamping*. Doctoral Dissertation. American Iron and Steel Institute. (Downloaded: December 2012). *UltraLight Steel Auto Body, Final Report*. www.autosteel.org.
- Banik, J., Lenze, F. J., Sikora, S., & Laurenz, R. (2011). *Tailored Properties - A Pivotal Question for Hot Forming*. Hot Sheet Metal Forming of High-Performance Steel, 3rd Int. Conference, Kassel, pp. 13-20.
- Bariani, P. F., Bruschi, S., Ghiotti, A., & Turetta, A. (2008). *Testing Formability in the Hot Stamping of HSS*. CIRP Annals, Manufacturing Technology, Vol. 57, pp. 265-268.
- Bleck, W., Papaefthymiou, S., & Frehn, A. (2004). *Microstructure and Tensile Properties in Dual Phase and Trip Steels*. Steel Research International, Vol. 75, Issue 11, pp.704-710.
- Bonacina, C., Cavallini, A., & Mattarolo, L. (1989). *Trasmissione del Calore*. Padova: CLEUP.
- Bosetti, P., Bruschi, S., Stöhr, T., Lechler, J., & Merklein, M. (2010). *Interlaboratory Comparison for Heat Transfer Coefficient Identification in Hot Stamping of High Strength Steels*. Proceedings of Esaform 2010.
- Casas, B., Latre, D., Rodriguez, N., & Valls, I. (2008). *Tailor Made Tool Materials for the Present and Upcoming Tooling Solutions in Hot Sheet Metal Forming*. 1st International Conference on Hot Sheet Metal Forming of High-Performance Steel, pp. 23–35.
- Dour, G., Dargusch, M., & Davidson, C. (2006). *Recommendations and Guidelines for the Performance of Accurate Heat Transfer Measurements in Rapid Forming Processes*. International Journal of Heat and Mass Transfer, Vol. 49, pp. 1773-1789.
- Field, F., Kirchain, R., & Roth, R. (October 2007). *Process Cost Modeling: Strategic Engineering and Economic of Materials Technologies*. JOM: the journal of the Minerals, Metals & Materials Society, Vol. 59, Issue 10, pp. 21-32.
- Galán, J., Samek, L., Verleysen, P., Verbeken, K., & Houbaert, Y. (2012). *Advanced High Strength Steels for Automotive Industry*. Revista de Metalurgia, Vol.48, Issue 2, pp. 118-131.
- George, R., Bardelcik, A., & Worswick, M. J. (November 2012). *Hot Forming of Boron Steels using Heated and Cooled Tooling for Tailored Properties*. Journal of Materials Processing Technology, Vol. 212, Issue 11, pp. 2386-2399.

- Ghosh, A., & Kikuchi, N. (1988). *Finite Element Formulation for the Simulation of Hot Sheet Metal Forming Processes*. International Journal of Engineering Science, Vol. 26, Issue 2, pp. 143-161.
- Hasan, S. H., Peet, J. M., Jalil, M. J., & Bhadeshia, H. K. (2011). *Heat Transfer Coefficients during Quenching of Steels*. Heat and Mass Transfer, Vol. 47, Issue 3, pp. 315-312.
- Helms, H., & Lambrecht, U. (2006). *The Potential Contribution of Light-Weighting to Reduce Transport Energy Consumption*. International Journal of Life Cycle Analysis, pp. 1-7.
- Hofmann, H., Mattissen, D., & Schaumann, T. W. (2009). *Advanced Cold Rolled Steels for Automotive Applications*. Steel Research International, Vol. 80, Issue 1, pp. 22-28.
- Kalpakjian, S., & Schmid, S. R. (2003). *Manufacturing Processes for Engineering Materials*. Prentice hall.
- Kang, J. H., Lee, K. O., & Kang, S. S. (2007). *Characterization of Cooling Heat Transfer for Various Coolant Conditions in Warm Forging Process*. Journal of Materials Processing Technology, Vol.184, pp. 338-344.
- Karbasian, H., & Tekkaya, A. E. (2010). *A Review on Hot Stamping*. Journal of Materials Processing Technology, 210, pp. 2103–2118.
- Lenze, F. J., Banik, J., & Sikora, S. (2008). *Applications of Hot Formed Parts for Body in White*. International Deep Drawing Research Group IDDRG, pp. 511–519.
- Madhusudana, C. V. (1996). *Thermal Contact Conductance*. Berlin: Springer-Verlag.
- Mangino, E., Carruthers, J. J., & Pitarresi, G. (2007). *The Future Use of Composite Materials in the Automotive Industry*. International Journal of Vehicle Design, Vol. 44,, pp. 211-232.
- Merklein, M., & Lechler, J. (2008). *Determination of Material and Process Characteristics for Hot Stamping Processes of Quenchenable Ultra High Strength Steels with Respect of Numerical Process Design*. Sae World Congress 2008.
- Merklein, M., & Lechler, J. (2009). *Determination of Material and Model Characteristics for Hot Stamping Processes of Quenchenable Ultra High Strength Steels with Respect to a FE-based Process Design* . SAE Int. Journal Mat. Manuf., Vol.1, Issue 1, pp. 411-426.
- Merklein, M., & Svec, T. (2012). *Hot Stamping: Manufacturing Functional Optimized Components*. Production Engineering, Vol. 7, Issue 2-3, pp. 141-151.
- Merklein, M., & Svec, T. (2012). *Prozessfenster zur Verarbeitung alternativer Stahlgüten im Presshärtprozess*. M. Merklein (Hrsg.): 7. Workshop Warmblechumformung, Bamberg, pp. 55-70.
- Merklein, M., Lechler, J., & Stöhr, T. (2008). *Characterization of Tribological and Thermal Properties of Metallic Coating for Hot Stamping Boron-Manganese Steels*. Proceedings of the 7th International Conference, Coatings in Manufacturing Engineering , pp. 219-227.



- Mori, K., Maki, S., & Tanaka, Y. (2005). *Warm and Hot Stamping of Ultra High Tensile Strength Steel Sheets*. CIRP Annals, Manufacturing Technology, Vol. 54, Issue 1, pp. 209-212.
- Moyer, J. M., & Ansel, G. S. (1975). *The Volume Expansion Accompanying the Martensite Transformation in Iron-Carbon Alloys*. Metallurgical and Materials Transactions A, Vol. 6, Issue 9, pp. 1785-1791.
- Naderi, M., Saeed-Akbari, A., & Bleck, W. (2008). *The Effects of Non-Isothermal Deformation on Martensitic Transformation in 22MnB5 Steel*. Material Science and Engineering A, pp. 445-455.
- Naderi, M. (2007). *Hot Stamping of High Strength Steels*. Doctoral Dissertation.
- Naderi, M., Durrenberger, L., Molinari, A., & Bleck, W. (2008). *Constitutive Relationship for 22MnB5 Boron Steel Deformed Isothermally at High Temperatures*. Material Science and Engineering A, Vol.478, Issue 1-2, pp.130-139.
- Neubauer, I., Hübner, K., & Wicke, T. (2008). *Thermo-Mechanically Coupled Analysis: the Next Step in Sheet Metal Forming Simulation*. 1st International Conference on Hot Sheet Metal Forming of High Performance Steel, Kassel, pp.275-283.
- Neugebauer, R., Altan, T., Geiger, M., Kleiner, M., & Sterzing, A. (2006). *Sheet Metal Forming at Elevated Temperatures*. CIRP annals - Manufacturing Technology, Vol. 55, Issue 2, pp. 793–816.
- Neugebauer, R., Göschel, A., Rautenstrauch, A., & Meza-García, E. (2011). *Influence of the Steel Alloy Composition on Phase Transition and its Applicability to Hot Forming Process*. Steel Research International, Special Edition, pp. 429-434.
- Rudiono, & Tomota, Y. (1997). *Application of the Secant Method to Prediction of Flow Curves in Multi-Microstructure Steels*. Acta Materialia, Vol.45, Issue 5, pp. 1923-1929.
- Shapiro, A. (2009). *Finite Element Modeling of Hot Stamping*. Steel Research International, Vol. 80, Issue 9, pp. 658-664.
- Shaw, J., & Zuidema, B. (2001). *New High Strength Steels Help Automakers Reach Future Goals for Safety, Affordability, Fuel Efficiency and Environmental Responsibility*. SAE Technical Paper 2001-01-3041.
- Stöhr, T., Lechler, J., & Merklein, M. (2009). *Investigation on Different Strategies for Influencing the Microstructural Properties with Respect to Partial Hot Stamping*. Hot Sheet Metal Forming of High-Performance Steel, pp. 273-281.
- Svec, T., & Merklein, M. (2011). *Tailored Tempering - Heat Transfer and Resulting Properties in Dependency of Tool Temperature*. 3rd International Conference on Hot Sheet Metal Forming of High-Performance Steels, pp. 21-29.
- Svec, T., & Merklein, M. (2012). *Tailored Tempering – FE-Simulation of Manufacturing Components with Local Adjusted Mechanical Properties*. Steel Research International; 14th International Conference Metal Forming, pp. 283-286.
- ThyssenKrupp Steel Europe. (Downloaded: December 2012a). *Complex-Phase Steels CP-W and CP-K*. www.thyssenkrupp-steel-europe.com.

- ThyssenKrupp Steel Europe. (Downloaded: December 2012b). *DP-W and DP-K Dual-Phase Steels*. [www.thyssenkrupp-steel-europe.com](http://www.thyssenkrupp-steel-europe.com).
- ThyssenKrupp Steel Europe. (Downloaded: Januar 2013). *Forming Properties of High-Strength and Ultra-High-Strength Multi-Phase Steels*. [www.thyssenkrupp-steel-europe.com](http://www.thyssenkrupp-steel-europe.com).
- Tondini, F., Borsetti, P., & Bruschi, S. (2009). *Inverse Analysis for HTC Identification*. Excerpt from the Proceedings of the COMSOL Conference.
- Tondini, F., Bosetti, P., & Bruschi, S. (2011). *Heat Transfer in Hot Stamping of High-Strength Steel Sheets*. Proceeding of the Institution of Mechanical Engineers, Part B: Journal of Engineering Manufacture, Vol. 225, pp. 1813-1824.
- Turetta, A. (2008). *Investigation of Thermal, Mechanical and Microstructural Properties of Quenchenable High Strength Steels in Hot Stamping Operations*. Doctoral Dissertation.
- Vandeputte, S., Vanderschhuern, D., Claessens, S., & Martinez, L. T. (2001). *Modern steel grades covering all needs of the automotive industry*. 9th International Conference on Steel Sheet Metal, pp. 405–414.
- Wang, C., Zhang, Y., Tian, X. W., Zhu, B., & Zhu, J. L. (2012). *Thermal Contact Conductance Estimation and Experimental Validation in Hot Stamping Process*. Science China Technological Sciences, Vol. 55, Issue 7, pp. 1852-1857.
- WorldAutoSteel. (Downloaded: December 2012). *Advanced High Strength Steel (AHSS) Application Guidelines*. [www.worldautosteel.org](http://www.worldautosteel.org).
- Xiaodong, Z., Zhaohui, M., & Li, W. (Downloaded: January 2013). *Current Status of Advanced High Strength Steel for Auto-making and its Development in Baosteel*. Baosteel research institute, published on: [www.baosteel.com](http://www.baosteel.com).